# PLAXIS

CONNECT Edition V21.00

User Defined Soil Models:

PM4Silt - A silt plasticity model for earthquake engineering [ULT]+[GSE]

Last Updated: January 18, 2021

Bentley®

# 1 Contents


1. Introduction ..... 4

1.1 Notation ..... 5

1.1. Basic equations of elasto-plasticity ..... 6

2. Model formulation ..... 7

2.1. Critical State Soil Mechanics framework ..... 7

2.2. Bounding, dilatancy, and yield surfaces ..... 11

1.1.1 Yield surface ..... 11

1.1.2 Dilatancy Surface (DS) ..... 11

1.1.3 Bounding Surface (BS) ..... 12

2.3. Fabric-dilatancy tensor ..... 13

2.4. Elasticity ..... 14

2.5. Hardening rule ..... 14

2.6. Flow rule ..... 15

1.1.4 Dilation: $\boldsymbol{D} < \mathbf{0}$ ..... 15

1.1.5 Contraction: $\boldsymbol{D} > \mathbf{0}$ ..... 16

2.7. Post-shaking analyses ..... 16

3. Model parameters and state variables ..... 18

3.1. Model Parameters ..... 18

1.1.6 Primary parameters ..... 20

1.1.7 Secondary parameters ..... 22

1.1.8 Post-shaking analysis parameters ..... 25

1.1.9 Alternative definition of a variable Undrained Shear Strength ..... 25

3.2. State variables ..... 26

4. Model response in undrained monotonic and cyclic loading conditions ..... 29

4.1. Simulations of stress-controlled CDSS tests and CRR vs N curves ..... 30

4.2. Normalized shear modulus reduction and damping ratio curves from PLAXIS SoilTest simulations ..... 33

5. A 1D site response analysis ..... 36

1.2 Results ..... 40

6. References ..... 44

APPENDIX ..... 46

A.1. Dilatancy expressions ..... 46

A.1.1 Dilating behavior ..... 46

A.1.2 Contracting behavior ..... 47

A.2. Anisotropic undrained strength for non-linear deformation analyses ..... 48

# 1. Introduction

The seismic performance of civil and geotechnical structures during earthquakes significantly depends on the undrained cyclic behavior of soils. Earth dams, river embankments, shallow foundations represent only a few examples for which accumulation of shear strains and generation of high excess pore water pressures induced by earthquakes can compromise the performance of the geotechnical systems. In both fine and coarse-grained soils, significant deformations are associated with the effective stress reduction and the pore pressures developed during ground motions. Specifically, in the case of low-plasticity silts and clays, the undrained behavior is influenced by the plastic characteristics of the soil and the mechanical response can manifest a transition between clay-like and sand-like behavior. Some differences between these two behavioral trends are schematically depicted in Figure 1. While clays are characterized by a relatively unique representation of the Normal Compression Locus (NCL), preserving also the parallelism between NCL and the Critical State Locus (CSL), the yielding of sands is associated with an infinite number of NCL, depending on the initial void ratio.

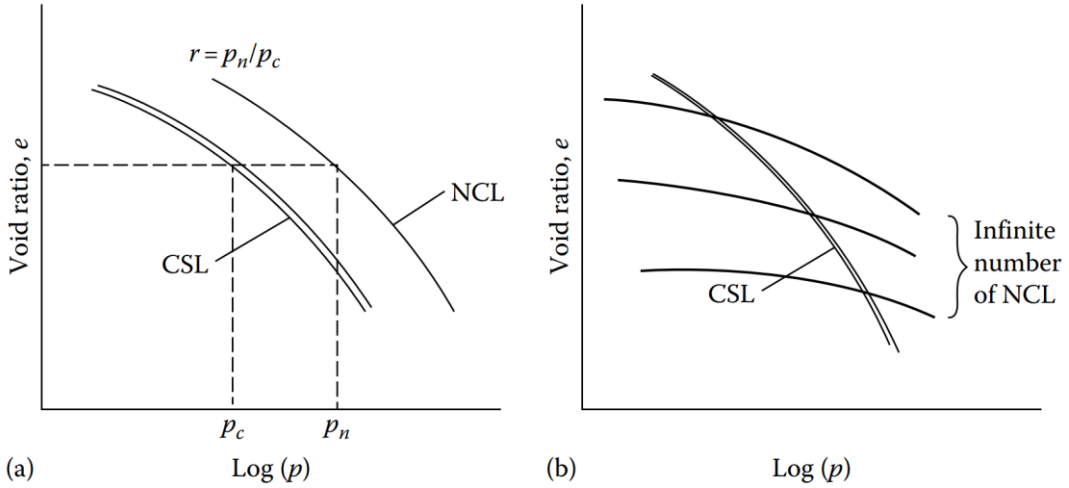


*Figure 1: Schematic idealization of clay-like and sand-like behaviors (figure after Jefferies and Been, 2015)*

Experimental evidence (Romero (1995), Boulanger et al. (2006), Dahl et al. (2014), Price et al. (2015), Price et al. (2017), Boulanger et al. (2016)) shows that the mechanical behavior of silts is strongly influenced by the plastic characteristics of the soil and that, for increasing values of the Plastic Index (PI), the tendency moves toward a clay-like behavior. Sand-like and clay-like characteristics of the undrained cyclic loading response are emphasized in Figure 2 where results of direct simple shear cyclic tests are shown for two normally consolidated silts having different PI. The difference between the two mechanical responses is appreciable by observing the minimum vertical effective stress reached at the end of the stress path and the evolution of the hysteresis loop which, for the non-plastic silt, are typical of sand-like behavior. Low-plasticity silts and clays can exhibit behaviors ranging from sand-like in some aspects to clay-like in others (Boulanger et al. (2006), Boulanger et al. (2018)). For instance, they can show stress-history normalized mechanical behavior (clay-like aspect) but still accumulate significant levels of excess pore water pressures during cyclic simple shear tests, as in sands (Dahl et al. (2014), Boulanger et al. (2019b)).

To cope with these complex features, a constitutive model has been recently formulated in Boulanger et al. (2018) which adapts a former model for sands (i.e. PM4Sand) to simulate the mechanical behavior of low-plasticity silts and clays under monotonic and cyclic loadings. This constitutive model, known in the literature as PM4Silt, has been implemented in PLAXIS 2D and is presented in the

following sections. The constitutive model formulation assumes the hypothesis of stress-history normalized undrained shear strength, therefore PM4Silt is not suited for non-plastic silts. For these silts, the former PM4Sand model, also available in PLAXIS 2D, should be preferred. After presenting the theoretical framework and explaining the meaning of the model parameters, some numerical analyses are reported to show the performance of the PM4Silt model.

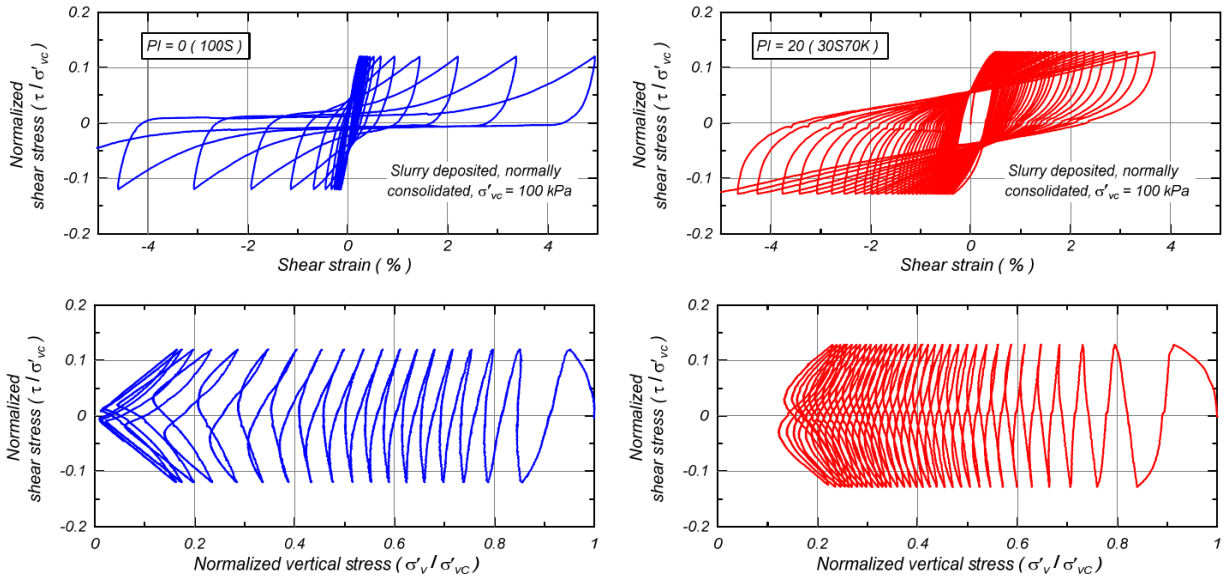


*Figure 2. Cyclic stress-strain and stress path plots for two different normally consolidated silts resulting from undrained cyclic direct simple shear tests (Boulanger et al. 2016)*

## 1.1 Notation

PM4Silt is a constitutive model formulated for two-dimensional problems and, for this reason, the stress tensor is defined as

$$\boldsymbol{\sigma} = \begin{pmatrix} \sigma_{xx} & \sigma_{xy} \\ \sigma_{xy} & \sigma_{yy} \end{pmatrix} \qquad \text{Eq. 1}$$

whereas the mean effective stress is

$$p = \frac{\sigma_{xx} + \sigma_{yy}}{2} \qquad \text{Eq. 2}$$

and the deviatoric stress tensor and the stress deviator are, respectively

$$\boldsymbol{s} = \boldsymbol{\sigma} - p\boldsymbol{I} = \begin{pmatrix} \sigma_{xx} - p & \sigma_{xy} \\ \sigma_{xy} & \sigma_{yy} - p \end{pmatrix}, \qquad q = \sqrt{2\,\mathbf{s}:\mathbf{s}} = \sqrt{2} \cdot |\boldsymbol{s}| \qquad \text{Eq. 3}$$

The symbol $\boldsymbol{I}$ represents the identity matrix ($\boldsymbol{I} = \delta_{ij}$ , $\delta_{ij}$ being the Kronecker's symbol) and the symbol "**:**" is used to indicate the inner product between tensors (i.e. $\boldsymbol{s}:\boldsymbol{s} = s_{ij}s_{ij}$) through which it is possible to define the Euclidean norm $|\boldsymbol{s}| = \sqrt{\boldsymbol{s}:\boldsymbol{s}}$. To characterize the hardening mechanism and the plastic flow of the model, the deviatoric stress ratio $\boldsymbol{r}$ and the related norm $\eta$ (i.e. the stress ratio) are defined respectively as

$$\boldsymbol{r} = \frac{\boldsymbol{s}}{p} = \begin{pmatrix} \frac{\sigma_{xx} - p}{p} & \frac{\sigma_{xy}}{p} \\ \frac{\sigma_{xy}}{p} & \frac{\sigma_{yy} - p}{p} \end{pmatrix}, \qquad \eta = \sqrt{2} \cdot |\mathbf{r}| \,. \tag{Eq. 4}$$

Similar definitions apply also for the strain tensor $\boldsymbol{\varepsilon}$ which is expressed as

$$\boldsymbol{\varepsilon} = \begin{pmatrix} \varepsilon_{xx} & \varepsilon_{xy} \\ \varepsilon_{xy} & \varepsilon_{yy} \end{pmatrix} \tag{Eq. 5}$$

where the volumetric strain is defined as

$$\varepsilon_v = \varepsilon_{xx} + \varepsilon_{yy} \tag{Eq. 6}$$

and the deviatoric strain tensor $\boldsymbol{e}$ (Boulanger et al. (2018))

$$\boldsymbol{e} = \boldsymbol{\varepsilon} - \frac{\varepsilon_v}{3}\boldsymbol{I} = \begin{bmatrix} \varepsilon_x - \frac{\varepsilon_v}{3} & \varepsilon_{xy} \\ \varepsilon_{xy} & \varepsilon_y - \frac{\varepsilon_v}{3} \end{bmatrix}. \tag{Eq. 7}$$

It is important to note that the stress invariants $p$ and $q$ are not the same as those shown by PLAXIS SoilTest and PLAXIS Output. If needed, these can be computed considering that $p$ and $q$ are defined as the center and the diameter of the effective stress Mohr's circle, respectively. In what follows, all stress measures are considered as effective and, for the sake of simplicity, the superscript " ' ", commonly used in soil mechanics notation, is omitted. Furthermore, the symbol " ˙ " is used to denote incremental quantities.

## 1.1. Basic equations of elasto-plasticity

The main equations of the elasto-plastic theory are recalled hereafter:

1. Hypothesis of strain additivity: $\dot{\boldsymbol{\varepsilon}} = \dot{\boldsymbol{\varepsilon}}^{el} + \dot{\boldsymbol{\varepsilon}}^{pl}$
2. Yield surface: $f(\boldsymbol{\sigma}, \boldsymbol{\alpha}) = 0$
3. Elastic relationship between elastic strain rate and stress rate: $\dot{\boldsymbol{\sigma}} = \boldsymbol{D^e} \cdot \dot{\boldsymbol{\varepsilon}}^{el}$
4. Flow rule: $\dot{\boldsymbol{\varepsilon}}^{pl} = \langle L \rangle \boldsymbol{R}$
5. Hardening rule $\dot{\boldsymbol{\alpha}} = \langle L \rangle \boldsymbol{\alpha}$

As usual, $\dot{\boldsymbol{\varepsilon}}^{el}$ and $\dot{\boldsymbol{\varepsilon}}^{pl}$ indicate the increments of the elastic and plastic parts of the strain tensor, the symbol $L$ stands for the plastic multiplier, $\boldsymbol{R}$ is the derivative of the plastic potential with respect to the current stress state, $\boldsymbol{D^e}$ is the elastic stiffness matrix and $\dot{\boldsymbol{\alpha}}$ is the rate of the hardening variable. $\langle \cdot \rangle$ denotes the Macaulay's brackets.

The elastoplastic stiffness matrix $\boldsymbol{D}^{ep}$ is obtained by enforcing the consistency conditions $\dot{f}(\boldsymbol{\sigma}, \boldsymbol{\alpha}) = 0$ to calculate the plastic multiplier $L$ and then by substituting this into the elastic relation used to define the stress increments. This tensor, which relates the increments of stress and total strain (i.e. $\dot{\boldsymbol{\sigma}} = [\, \boldsymbol{D^{ep}} \,]\dot{\boldsymbol{\varepsilon}}$), is defined as

$$\boldsymbol{D}^{ep} = \boldsymbol{D}^e - \langle L \rangle \boldsymbol{D}^e \boldsymbol{R}, \tag{Eq. 8}$$

with the plastic multiplier expressed as

$$L = \left[ \frac{(\mathbf{D}^e \boldsymbol{L})^T}{K_P + (\boldsymbol{D}^e \boldsymbol{R}) \boldsymbol{L}^T} \right] \dot{\boldsymbol{\varepsilon}} \,. \tag{Eq. 9}$$

In Eq. 9, $\boldsymbol{L}$ represents the gradient $\partial f / \partial \sigma_{ij}$ and $K_P$ the hardening modulus defined as

$$K_p = -\left(\frac{\partial f}{\partial \boldsymbol{\alpha}}\right)\boldsymbol{\alpha}\,. \qquad \textit{Eq. 10}$$

By substituting Eq. 9 into Eq. 8, it is possible to rewrite the expression of the elasto-plastic tensor in its final form as

$$\boldsymbol{D^{ep}} = \left[\boldsymbol{D}^e - \frac{(\boldsymbol{D}^e\boldsymbol{R})(\boldsymbol{D}^e\boldsymbol{L})^T}{K_P + (\boldsymbol{D}^e\boldsymbol{R})^T\boldsymbol{L}}\right] \qquad \textit{Eq. 11}$$

# 2. Model formulation

## 2.1. Critical State Soil Mechanics framework

PM4Silt is an elasto-plastic constitutive model formulated within the theory of Critical State Soil Mechanics (CSSM) and can be used to simulate the cyclic response of silty soils. In this framework, the projection of the Critical State Locus (CSL) in the p-q plane is defined by the following equation

$$q_{cs} = M \cdot p_{cs} \qquad \textit{Eq. 12}$$

$M$ being the slope of the CSL in the p-q plane which is related to the constant volume friction angle $\varphi_{cv}$ through

$$M = 2 \cdot \sin(\varphi_{cv}). \qquad \textit{Eq. 13}$$

The projection of the CSL in the $e - \ln(p)$ is expressed as

$$e_{cs} = \Gamma - \lambda \ln\left[101.3\left(\frac{p_{cs}}{p_{atm}}\right)\right] \qquad \textit{Eq. 14}$$

where $p_{atm}$ is the atmospheric pressure, $\lambda$ is the slope of the CSL and $\Gamma$ represents the void ratio at the reference mean stress $p = 1\ kPa$. PM4Silt adopts the state parameter $\xi$ (Been et al. (1985)) to distinguish states looser and denser than the Critical State (CS), defined by

$$\xi = e - e_{cs}\,, \qquad \textit{Eq. 15}$$

$e$ being the current void ratio and $e_{cs}$ the void ratio on the CSL computed with the current mean pressure. In PM4Silt the undrained strength at Critical State $S_u$ is given as an input and can be prescribed through two alternative procedures: *(i)* by assigning explicitly the value of $S_u$, *(ii)* by providing the undrained strength ratio at CS as

$$S_{u,ratio} = \frac{S_u}{\sigma_{vc}}, \qquad \textit{Eq. 16}$$

$\sigma_{vc}$ being the vertical effective stress at consolidation, usually assumed equal to the initial vertical effective stress. According to Eq. 16, $S_u$ is then calculated as $S_u = \sigma_{vc} \cdot S_{u,ratio}$. Consistently with other constitutive models based on CSSM, $\Gamma$ is not reported as a parameter but it is computed by using the undrained resistance at CS. As a result, considering the relation between the stress deviator and the undrained strength (i.e. $q_{cs} = 2 \cdot S_u$), the mean stress at critical stress is

$$p_{cs} = 2\,S_u/M\,. \qquad \textit{Eq. 17}$$

By combining Eq. 14 and Eq. 17 and by assuming a constant void ratio, the intercept $\Gamma$ can be calculated as

$$\Gamma = e_0 + \lambda \cdot \ln\left[101.3\left(\frac{2}{M}\frac{S_u}{p_{atm}}\right)\right], \qquad \text{Eq. 18}$$

or, equivalently, as

$$\Gamma = e_0 + \lambda \cdot \ln\left[101.3\left(\frac{2}{M}\frac{\sigma_{vc}\, S_{u,ratio}}{p_{atm}}\right)\right]. \qquad \text{Eq. 19}$$

Based on the hypothesis that $e_{cs} \equiv e_0$, this procedure enables to accommodate the CSL according to the undrained strength $S_u$ and the initial void ratio which represents a further input of the model. Eq. 18 and Eq. 19 are equivalent if a single element of soil is considered but they imply a different representation of the CSL in the case of constant void ratio and variable vertical effective stresses. In this context, while prescribing a unique value of $S_{u,ratio}$ involves different positions of the CSL and enables to consider the dependency of $S_u$ on the initial vertical effective stress (Figure 3(a)), assigning $S_u$ as an input is equivalent to have a unique representation of the CSL in the compressibility plane $e - ln(p)$ (Figure 3 (b)). As a result, a unique value of the parameter $S_u$ implies a different initial state of the soil (normally or over-consolidated in Figure 3 (b)), whereas, on the contrary, assigning $S_{u,ratio}$ is valid for a specific OCR and a given $K_0$.

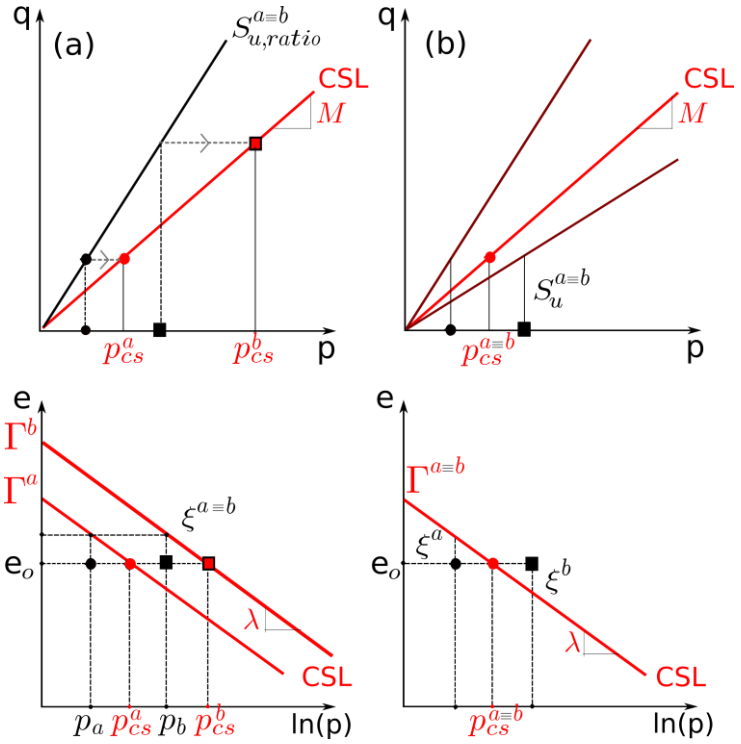


*Figure 3. Schematic representation of the CSL based on two different choices of the input parameters for the same initial conditions: (a) case corresponding to a prescribed $S_{u,ratio}$, (b) case corresponding to a prescribed $S_u$. For the sake of simplicity, in both figures, an isotropic initial stress state is considered (i.e. $p_a$ and $p_b$)*

As the approach considered to accommodate the CSL in the compressibility plane (Figure 3) is based on the constitutive framework characteristics of clay-like behavior, PM4Silt is not suited for purely non-plastic silts. Although in the model the distinction between normally- and over-consolidated states cannot be explicitly simulated due to the lack of a cap, in this framework the effect of the OCR on the undrained strength as well as on the cyclic resistance by using $S_{u,ratio}$ should be considered in the calibration. In clay-like materials, the undrained strength ratio can be used to express $S_u$ as an analytical function of the initial consolidation pressure and the intrinsic properties of the soil. For this purpose, we can define the following ratio, valid for normally consolidated soils,

$$\alpha^{nc} = \frac{p_{cs}}{p_o} = exp\left(\frac{\Gamma - N}{\lambda}\right) < 1\,, \qquad \text{Eq. 20}$$

and, by combining Eq. 20 and Eq. 12, it is possible to obtain the expression of the undrained strength for a given soil and a given value of the initial stress as

$$S_u = \frac{q_{cs}}{2} = \frac{M}{2} p_{cs} = \left(\frac{M\,\alpha^{nc}}{2}\right) p_o\,. \qquad \text{Eq. 21}$$

The effect of having $\alpha^{nc} < 1$ is depicted in Figure 4 showing a qualitative stress path in undrained conditions. The same logic can be applied to over-consolidated soils defining the ratio $\alpha^{oc} = \alpha^{nc}\, OCR^{m}$, with $m$ expressed as a function of the compressibility properties of the soil, which gives

$$S_u = \frac{q_{cs}}{2} = \frac{M}{2} p_{cs} = \left(\frac{M\,\alpha^{oc}}{2}\right) p_{curr}\,. \qquad \text{Eq. 22}$$

As a result, by assuming an isotropic initial stress state (i.e. $p_{curr} \equiv \sigma'_{vc}$), Eq. 21 (or Eq. 22) can be rearranged to relate $\alpha$ and $S_{u,ratio}$, that is

$$\frac{S_u}{\sigma'_{vc}} = \frac{M}{2}\alpha = S_{u,ratio}\,, \qquad \text{Eq. 23}$$

where $\alpha \equiv \alpha^{nc}$ or $\alpha \equiv \alpha^{oc}$ for normally consolidated and over-consolidated soils, respectively. The relationship between OCR and the normalized undrained strength, deduced by using the analytical framework of CSSM, is also depicted in Figure 5. It is important to remark that $M$ is commonly measured by means of triaxial compression tests and, consequently, for other types of stress paths, the $S_{u,ratio}$ calculated with Eq. 23 should be decreased to account for a reduced value of $M$ at CS.

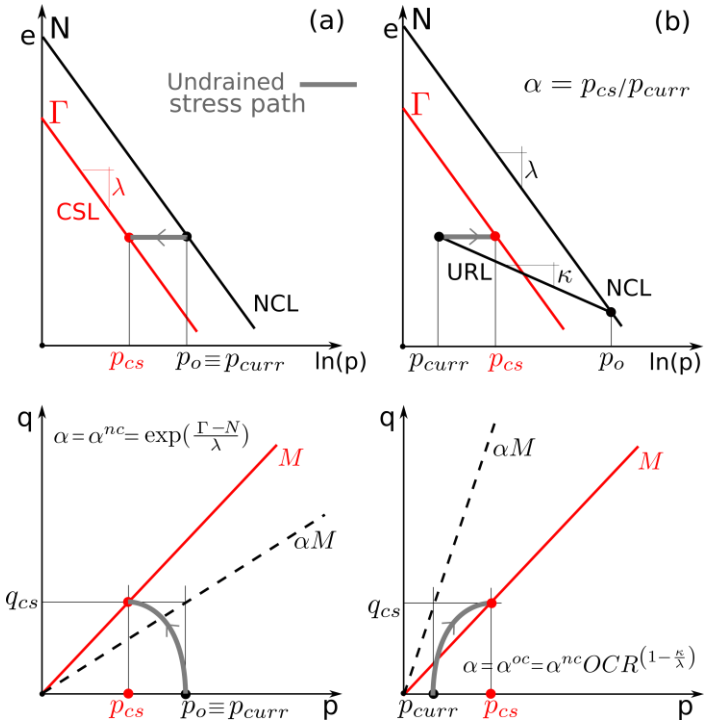


*Figure 4. Schematic representation of the effective stress paths of two samples of a clay during undrained triaxial compression: (a) case of an initial normally consolidated state (b) case of an initial over-consolidated state.*

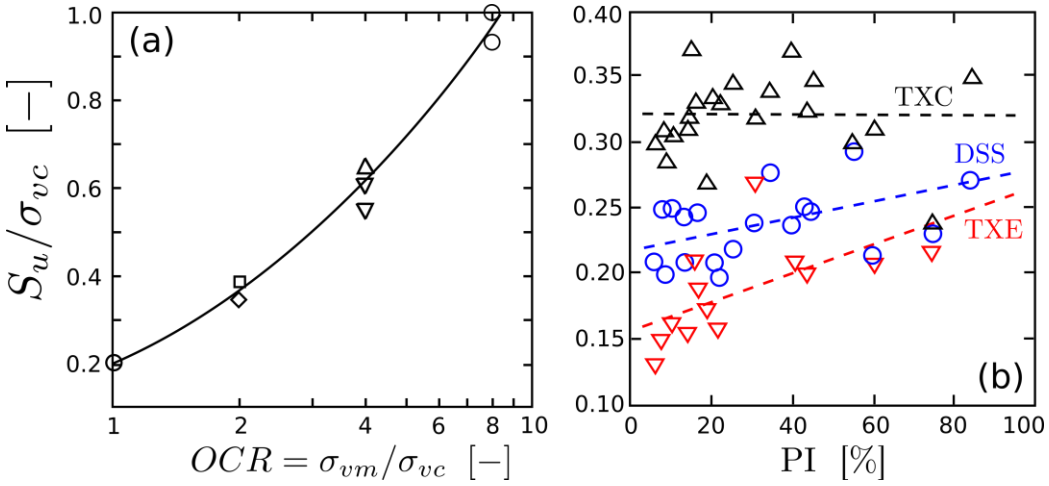


Figure 5. (a) *Normalized undrained shear strength versus OCR in direct simple shear tests for the Boston Blue clay (figure after Ladd et al. (1974)). (b) Differences in undrained strength for normally consolidated silts and clays with different plasticity index (PI) (figure from Ladd et al. (2003)).*

A further limitation of Eq. 23 is related to anisotropic consolidation processes which can have an influence on the undrained strength ratio. Especially if an analysis of existing geotechnical structures is required, the dependency of $S_{u,ratio}$ on $K_o$ should be accounted to obtain a realistic dependency of $S_u$ on the initial vertical effective stress. To overcome this limitation and account for a $S_u$ that varies for each stress point, the method proposed by Montgomery et al. (2014), extending the procedure described in Duncan et al. (2005) for limit equilibrium analyses, has been proposed in the current implementation of PM4Silt. This method consists of calculating the shear stress $\tau_{ff,K_c}$ on the eventual failure plane at undrained failure for general consolidation condition (with $K_c = \sigma_{1c}/\sigma_{3c}$ indicating the consolidation stress ratio) through a linear interpolation between the undrained strengths for consolidation at $K_c = 1$ and $K_c = K_f$, i.e.

$$S_u \equiv \tau_{ff,K_c} = \tau_{ff,(K_c=1)} + \left[\frac{\tau_{ff,(K_c=K_f)} - \tau_{ff,(K_c=1)}}{K_f - 1}\right](K_c - 1). \qquad \text{Eq. 24}$$

In this equation, $K_c$ is the consolidation stress ratio $K_c = \sigma_{1c}/\sigma_{3c}$ for generic conditions of consolidation whereas $K_f$ is the highest possible $K_c$ ($f$ denoting failure). In Eq. 24, the undrained strength, although should be $S_u = \tau_{ff,K_c}/cos(\varphi_{cs})$, it has been defined as the stress on the failure plane as suggested in Boulanger (2019) where this method is used in nonlinear dynamic analysis of a compacted earth dam performed with PM4Silt. The two shear stresses on the eventual failure planes (i.e. $\tau_{ff,K_c=1}$ and $\tau_{ff,K_c=K_{cf}}$) are computed respectively as

$$\tau_{ff,(K_c=1)} = d_R + \sigma_{fc} \cdot tan(\psi_R)\,, \qquad \text{Eq. 25}$$

$$\tau_{ff,(K_c=K_f)} = c_c + \sigma_{fc} \cdot tan(\phi_c) \qquad \text{Eq. 26}$$

where $c_c$, $\phi_c$ and $d_R$, $\psi_R$ are parameters that can be computed from ICU Triaxial tests. To compute these parameters no additional tests are required but only a different interpretation of the results. The two parameters indicated with $c_c$, $\phi_c$ are the intercepts and slopes of the effective stress failure envelope (usually indicated as $c'$, $\phi'$ ). In the context of the method, $c_c$, $\phi_c$ are used to compute the undrained strength for the case of consolidation at $K_c = K_f$ (Eq. 25). The parameters $d_R$, $\psi_R$ can be obtained by plotting the undrained shear strength (considered as $\tau_{ff,(K_c=1)}$) versus the initial mean effective stress at consolidation and evaluating the intercept and slope of the linear fit of the data. The computation of $K_c$ in Eq. 24 is performed internally for every single stress point based on the

initial effective stress. The four parameters represent only an alternative way to prescribe a variable $S_u$ throughout the domain. Additional mathematical details about this approach are provided in Appendix A.2.

## 2.2. Bounding, dilatancy, and yield surfaces

PM4Silt incorporates the concepts of bounding and dilatancy stress ratio surfaces, consistently with the former approach proposed in Dafalias et al. (2004). The bounding and dilatancy stress ratios indicated as $M^b$ and $M^d$ respectively, depend on the current state of the material and converge to the stress ratio $M$ when the stress response approaches the CS. However, being PM4Silt defined for 2D problems, there is no introduction of a dependency on the Lode angle in the plastic functions of the model.

### 1.1.1 Yield surface

The yield surface is formulated as a cone in the stress space, defined as

$$f = [(\boldsymbol{s} - p\boldsymbol{\alpha}) : (\boldsymbol{s} - p\boldsymbol{\alpha})]^{1/2} - \sqrt{1/2}\; p\, m = 0\,. \qquad \text{Eq. 27}$$

The tensor $\boldsymbol{\alpha}$ is the back-stress ratio tensor which represents the hardening variable of the model and defines the position of the axis of the yield surface. $m$ is the semi-amplitude of the cone and it is assumed to be constant and equal to $m = 0.01$ (Figure 6). The hardening modulus and the elasto-plastic tensor are calculated using the tensor $\boldsymbol{n}$ representing the deviatoric unit normal to the yield surface, i.e.

$$\boldsymbol{n} = \frac{\partial f}{\partial \boldsymbol{s}} = \sqrt{2}\left[\frac{\boldsymbol{r} - \boldsymbol{\alpha}}{m}\right]. \qquad \text{Eq. 28}$$

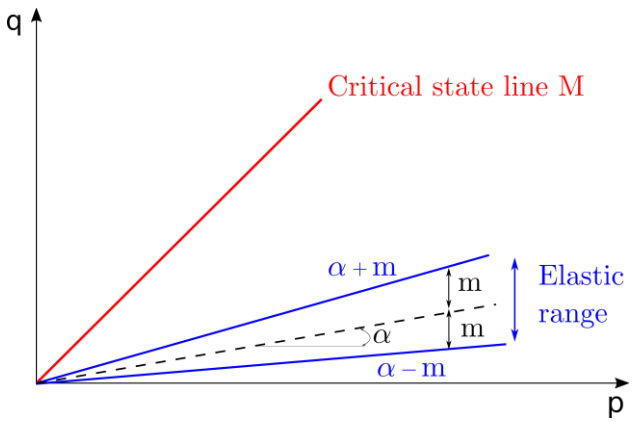


Figure 6. *Schematic representation of the yield surface formulated in PM4Silt.*

### 1.1.2 Dilatancy Surface (DS)

The dilatancy stress ratio $M^d$ is expressed as

$$M^d = M \cdot exp\left(n^d \frac{\xi}{\lambda}\right), \qquad \text{Eq. 29}$$

$n^d$ being a positive parameter. According to the sign of ξ, the DS lies below or above the CS line (Figure 7), that is negative or positive values of ξ are associated with material states denser or looser than CS, respectively. Analogously to the bounding, the dilatancy stress ratio is considered to define the dilatancy back-stress ratio tensor in terms of

$$\boldsymbol{a}^d = \sqrt{\frac{1}{2}}\left(M^d - m\right)\boldsymbol{n}\,. \qquad \text{Eq. 30}$$

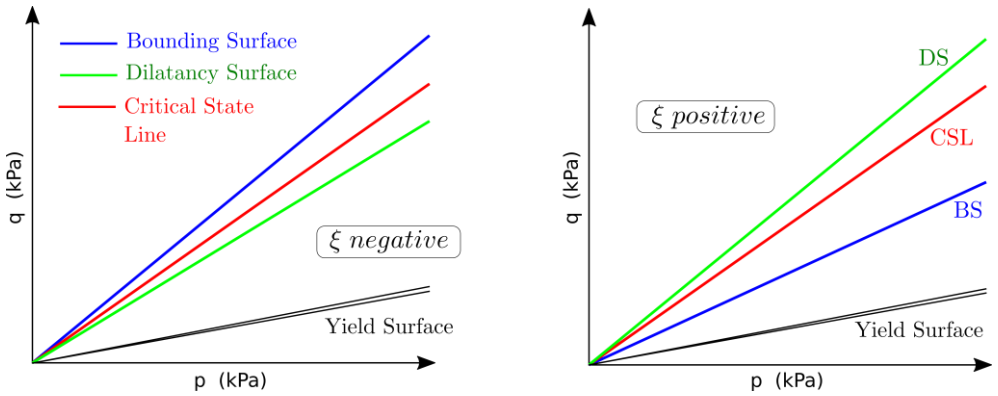


Figure 7. *Schematic representation of bounding and dilatancy stress ratios for a given value of the state parameter: negative and positive ξ denote soils denser and looser than CS, respectively.*

### 1.1.3 Bounding Surface (BS)

The bounding stress ratio $M^b$ is defined differently for states looser ("wet" side) and denser ("dry" side) than CS, i.e. negative or positive values of the state parameter, respectively. For the looser case, it is

$$M^b = M \cdot exp\left(-n^{b,wet}\frac{\xi}{\lambda}\right) \quad for\ \xi > 0, \qquad \text{Eq. 31}$$

where $n^{b,wet}$ is a positive parameter of the model employed to have the bounding stress ratio smaller than the CS (that is $M^b < M$ for $\xi > 0$, see Figure 7). On the "dry" side $M^b$ is expressed as

$$M^b = M \cdot \left(\frac{1 + C_{Mb}}{\frac{p}{p_{cs}} + C_{Mb}}\right)^{n^{b,dry}} \quad for\ \xi < 0, \qquad \text{Eq. 32}$$

$$C_{Mb} = \frac{1}{\left(\frac{M^{b,max}}{M}\right)^{1/n^{b,dry}} - 1}, \qquad \text{Eq. 33}$$

$$M^{b,max} = 2 \cdot \sin(\varphi_{max})\,, \qquad \text{Eq. 34}$$

$n^{b,dry}$ being a positive parameter of the model. $\varphi_{max}$ is a constant and is equal to $\varphi_{max} = 60°$. Eq. 31 and Eq. 32 are used to define the image of the back-stress ratio tensor through

$$\boldsymbol{a}^b = \sqrt{\frac{1}{2}}\left(M^b - m\right)\boldsymbol{n}\,. \qquad \text{Eq. 35}$$

The abovementioned equations show that, for a given value of ξ, the DS and BS are represented by straight lines in the *p-q* plane, having slopes corresponding to $M^d$ and $M^b$, respectively. A representation of these surfaces for a fixed value of the void ratio is shown in Figure 8. In this figure, it is possible to observe that the DS, BS, and CS intersect each other at the specific value of the mean stress for which the state parameter vanishes, corresponding to $p \equiv p_{cs}$. The effect of the parameters

$n^{b,wet}$ and $n^{b,dry}$ on the trend of the Bounding line, respectively on the "wet" and "dry side", is also shown in Figure 8.

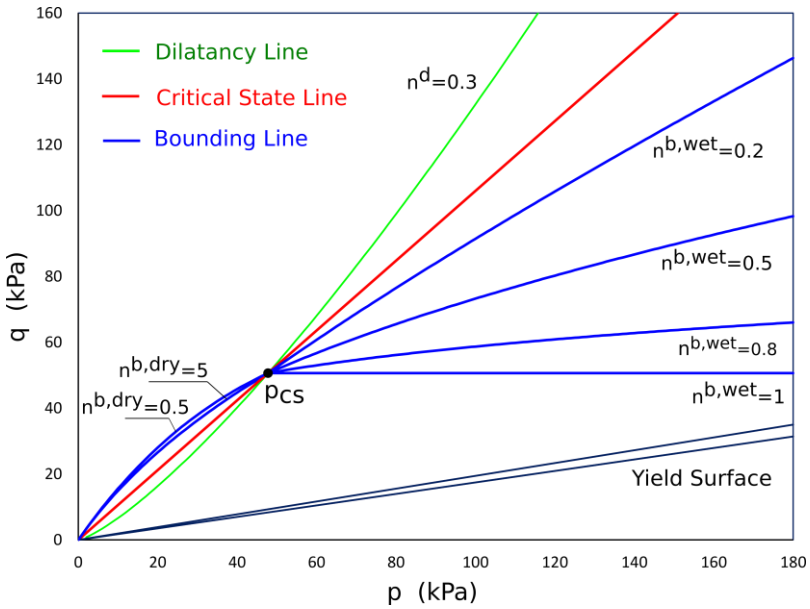


Figure 8. *Schematic representation of the bounding and dilatancy stress ratios for a given void ratio.*

Consistently with former bounding surface models, the value of the initial back-stress ratio tensor is tracked at every change in loading direction, identified by the condition $(\boldsymbol{\alpha} - \boldsymbol{\alpha}_{ini}) : \boldsymbol{n} < \boldsymbol{0}$, and used to compute the hardening modulus. Specifically, the values of $\boldsymbol{\alpha}_{ini}$ are updated to the current $\boldsymbol{\alpha}$ when the first inversion of the loading direction is detected. In subsequent inversions of the stress path, this tensor is used to define the tensor $\boldsymbol{\alpha}_{ini,p}$ (i.e. $\boldsymbol{\alpha}_{ini,p} \equiv \boldsymbol{\alpha}_{ini}$) while the current value of $\boldsymbol{\alpha}$ is assigned to $\boldsymbol{\alpha}_{ini}$. In this manner, the back-stress ratio tensor is stored at the last two loading reversals of the cyclic loading. The model defines also a tensor $\boldsymbol{\alpha}_{ini}^{app}$ which is introduced to avoid unrealistic stiffness during small cycles of loading/unloading.

## 2.3. Fabric-dilatancy tensor

In the model proposed in Dafalias et al. (2004), the fabric-dilatancy tensor $\boldsymbol{z}$ was introduced to take into account the effect of the previous straining on the mechanical response of sands. Conrrespondly, the incremental equation adopted in PM4Silt is defined as

$$\dot{\boldsymbol{z}} = -\frac{C_z}{1 + \left\langle \frac{z_{cum}}{2z_{max}} - 1 \right\rangle} \frac{\langle -\dot{\varepsilon}_v^{pl} \rangle}{D} (z_{max}\boldsymbol{n} + \boldsymbol{z}) \qquad \textit{Eq. 36}$$

where $D$ is the dilatancy, $z_{max}$ is a parameter defining the range of values that $\boldsymbol{z}$ can attain, $C_z$ is a parameter controlling the rate of evolution of $\boldsymbol{z}$, and $z_{cum}$ is the cumulative value of the absolute changes in $\boldsymbol{z}$ which are computed according to $\dot{z}_{cum} = |\dot{\boldsymbol{z}}|$. In Eq. 36 the Macauley's brackets in the ratio $\langle -\dot{\varepsilon}_v^{pl} \rangle / D$ implie a variation of the fabric tensor only during dilating behavior, being this the reason for this tensor to be denominated "fabric-dilatancy", although the same ratio shows that (as opposed to the model in Dafalias et al. (2004)) $\dot{\boldsymbol{z}}$ depends only on the modulus of the deviatoric plastic strain rate. By observing Eq. 36, it is also worth remarking that the rate of evolution of $\boldsymbol{z}$ tends to vanish for large values of $z_{cum}$ (i.e. $z_{cum} \ll z_{max}$), thus having the tensor $\boldsymbol{z}$ characterized by constant values.

## 2.4. Elasticity

An isotropic hypo-elastic model is considered to simulate the elastic behavior of PM4Silt. The elastic shear modulus depends on (i) the mean effective stress, (ii) the stress ratio (iii) the fabric tensor and is defined as

$$G = G_0 p_{atm} \left(\frac{p}{p_{atm}}\right)^{n_G} C_{SR} \left[\frac{1 + \left(\frac{z_{cum}}{z_{max}}\right)}{1 + \left(\frac{z_{cum}}{z_{max}}\right) C_{GD}}\right]. \quad \text{Eq. 37}$$

In this equation $G_0$ and $n_G$ are two parameters related to the dependency of the small strain shear modulus on the mean effective stress. $C_{GD}$ is a parameter controlling the shear stiffness degradation at large values of $z_{cum}$ while $C_{SR}$ provides the dependency on the stress ratio through

$$C_{SR} = 1 - C_{SR,0} \cdot \left(\frac{M}{M^b}\right)^{m_{SR}}, \quad \text{Eq. 38}$$

where $m_{SR} = 4$ and $C_{SR,0} = 0.5$. As the Poisson's ratio $\nu$ is given as an input parameter, the bulk modulus is calculated as

$$K = \frac{2}{3}\left(\frac{1+\nu}{1-2\nu}\right) G. \quad \text{Eq. 39}$$

In the formulation of $G$, the dependency on the current void ratio, formerly proposed in Dafalias et al. (2004), has been replaced by introducing a dependency on the fabric-dilatancy tensor (i.e. by introducing the variables $z_{cum}/z_{max}$) and the ratio $M/M^b$. The advantage of using these complex dependencies in the formulation of the shear modulus results in better modeling of the stress-strain response for soils susceptible to flow liquefaction. In particular, the definition of the shear modulus has three main consequences: *(i)* the bulk modulus gradually decrease as $z_{cum}$ increases, *(ii)* the decreasing trend of $G$ after phase transformation involves a decreasing trend of the strain hardening and (*iii*) the ability to better approximate the hysteretic stress-strain response during cyclic softening (Boulanger et al. (2018)). It is worth remarking that the stress component $\sigma_{zz}$ has no influence on the plastic mechanisms of the model therefore it is computed using a linear elastic relation and the hypothesis of plane-strain conditions, that is $\dot{\sigma}_{zz} = \nu\dot{\sigma}_{xx} + \nu\dot{\sigma}_{yy}$.

## 2.5. Hardening rule

The yield surface of PM4Silt evolves according to a rotational hardening mechanism governed by an incremental variation of the back-stress ratio tensor in line with the hardening rule defined in Dafalias et al. (2004), which is

$$\dot{\boldsymbol{\alpha}} = \langle L \rangle h\left(\boldsymbol{\alpha}^b - \boldsymbol{\alpha}\right), \quad \text{Eq. 40}$$

$h$ being the hardening coefficient, a function of the plastic modulus $K_p$, defined as

$$h = \frac{K_p}{p \cdot (\boldsymbol{\alpha^b} - \boldsymbol{\alpha}) : \boldsymbol{n}}, \quad \text{Eq. 41}$$

where

$$K_p = h_0 \cdot G \cdot \frac{\left[(\boldsymbol{\alpha}^b - \boldsymbol{\alpha}) : \boldsymbol{n}\right]^{0.5}}{\left[exp\left((\boldsymbol{\alpha} - \boldsymbol{\alpha}_{ini}^{app}) : \boldsymbol{n}\right) - 1\right] + C_{\gamma 1}} \cdot \frac{C_{rev} C_{k\alpha}}{1 + C_{Kp}\left(\frac{z_{peak}}{z_{max}}\right) \langle (\boldsymbol{\alpha^b} - \boldsymbol{\alpha}) : \boldsymbol{n} \rangle \sqrt{1 - C_{zpk2}}}. \quad \text{Eq. 42}$$

In this last expression, it appears $h_0$ which is a further parameter of the model. Moreover, $C_{rev}$ and $C_{k\alpha}$ contain a dependency on the back-stress ratio history and the fabric history during the loading process, whereas $z_{peak} = max(\,|\boldsymbol{z}|/\sqrt{2}, z_{peak})$ is used to track the history of $\boldsymbol{z}$ and $C_{\gamma 1}$is fixed and equal to $h_0/100$. Further explanations and mathematical details about these variables can be found in Boulanger et al. (2018) and Boulanger et al. (2017).

## 2.6. Flow rule

Plastic strain increments can be calculated by using the classical flow rule

$$\dot{\boldsymbol{\varepsilon}}^{pl} = \langle L \rangle \boldsymbol{R} \qquad \textit{Eq. 43}$$

where $L$ indicates the plastic multiplier and $\boldsymbol{R}$ is the derivative of plastic potential.

$$\boldsymbol{R} = \boldsymbol{n} + \frac{1}{3} D \boldsymbol{I} \qquad \textit{Eq. 44}$$

The direction of the plastic flow can be decomposed into two components defining the deviatoric and volumetric plastic strain increments

$$\dot{\varepsilon}_v^{pl} = \frac{2}{3} \langle L \rangle D \qquad \textit{Eq. 45}$$

$$\dot{\boldsymbol{e}}^{pl} = \langle L \rangle \boldsymbol{n} \qquad \textit{Eq. 46}$$

A synthetic description of the mathematical expressions implemented to define the dilatancy *D* for the two cases of dilation and contraction is presented below and is schematically depicted in Figure *9*.

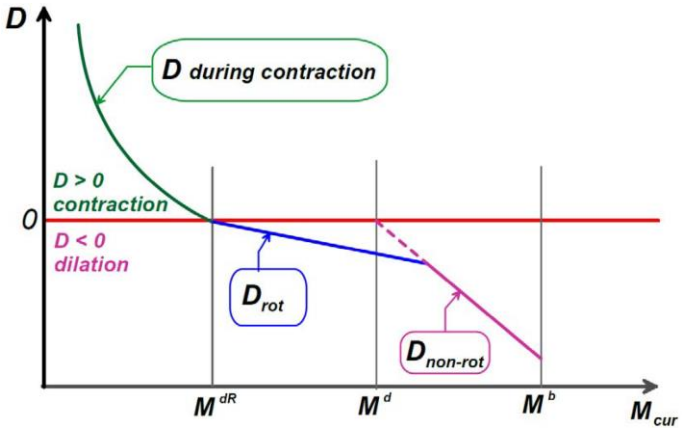


Figure 9. *Schematic representation of the dilatancy function considered in PM4Silt (figure after Boulanger et al. (2018)).*

### 1.1.4 Dilation: $\boldsymbol{D < 0}$

Dilation occurs every time $(\boldsymbol{\alpha}^{dR} - \boldsymbol{\alpha})\colon \boldsymbol{n} < \boldsymbol{0}$. In this case, the value of $D$ is defined by comparing the following two quantities

$$D_{rot} = A_d \cdot \frac{\langle -\boldsymbol{z}\colon \boldsymbol{n} \rangle}{\sqrt{2} z_{max}} \cdot \frac{(\boldsymbol{\alpha}^{dR} - \boldsymbol{\alpha})\colon \boldsymbol{n}}{C_{DR}}, \qquad \textit{Eq. 47}$$

$$D_{non-rot} = -A_d \langle\, -(\boldsymbol{a}^{d} - \boldsymbol{a})\colon \boldsymbol{n} \,\rangle \qquad \textit{Eq. 48}$$

$\boldsymbol{a}^{dR}$ is the back-stress ratio tensor for the rotated dilatancy surface and $A_d$ is a function depending on the fabric tensor and the deviatoric unit tensor $\boldsymbol{n}$. Both $\boldsymbol{a}^{dR}$ and $A_d$ are characterized by complex

mathematical expressions which are reported in Appendix A.1 (A1. 3). The definition of $A_d$ implies the introduction of two further parameters, $A_{d0}$ and $C_\varepsilon$, enabling a better fit of the experimental data.

It is worth mentioning that in PM4Silt dilation occurs also for mean stresses $p \leq 2\,p_{min}$, where $p_{min}$ is an internal parameter of the model and can be set in two ways as explained in Section 3.1 (Eq. 64 and Eq. 65). In this particular case, it is

$$D = -3.5A_{do}\langle M^b - M^d\rangle \cdot \left(\frac{2p_{min} - p}{p_{min}}\right). \qquad \text{Eq. 49}$$

### 1.1.5 Contraction: $\boldsymbol{D > 0}$

In the case of contraction, it is

$$D = A_{dc}[(\boldsymbol{\alpha} - \boldsymbol{\alpha}_{in}^{app}):\boldsymbol{n} + C_{in}]^2 \cdot \left[\frac{(\boldsymbol{\alpha}^d - \boldsymbol{\alpha}):\boldsymbol{n}}{(\boldsymbol{\alpha}^d - \boldsymbol{\alpha}):\boldsymbol{n} + C_D}\right] C_{p,min} \qquad \text{Eq. 50}$$

The value of $C_D$ is usually assumed equal to 0.10, while the function $A_{dc}$ is defined as

$$A_{dc} = \frac{A_{d0}}{h_p} \cdot \left[\frac{1 + \langle \boldsymbol{z}:\boldsymbol{n}\rangle}{C_{dz}C_{wet}}\right] \qquad \text{Eq. 51}$$

where

$$h_p = h_{p0} \cdot exp\left[-0.7 + 0.2\left(3 - \frac{\xi}{\lambda}\right)^2\right] \qquad \text{Eq. 52}$$

$h_{p0}$ and $A_{d0}$ being model parameters that can be evaluated during the calibration process to better fit the experimental trend of the Cyclic Resistance Ratio (CRR). The mathematical expressions of the variables $C_{in}$, $C_{p,min}$, $C_{dz}$ and $C_{wet}$ are reported in Appendix A.1. (and in Boulanger et al. (2018)).

## 2.7. Post-shaking analyses

Although PM4Silt is not suited for simulating the consolidation process due to the lack of a cap, it uses a pragmatic approach to simulate consolidation phenomena after strong shaking in cyclically softened silts/clays without underestimating the volumetric strains. The approach considers a reduction of the stiffness through

$$G_{post-shaking} = F_{consol}G \qquad \text{Eq. 53}$$

where the factor $F_{consol}$ is defined as

$$F_{consol} = 1 - \left(1 - \frac{G_{c,min}}{G}\right)\left\langle 1 - \frac{M_{curr}}{M^d}\right\rangle^{0.25} \qquad \text{Eq. 54}$$

being

$$G_{c,min} = 8\left(\frac{p}{\lambda}\right) \cdot \left[\frac{1}{1 + (CG_{consol} - 1)\cdot\left(\frac{z_{cum}}{z_{cum} + z_{max}}\right)}\right], \qquad \text{Eq. 55}$$

$CG_{consol}$ being a parameter controlling the amount of shear modulus degradation when $z_{cum}$ tends to large values. If $z_{cum}$ is small, $G_{c,min}$corresponds to the shear modulus connected to the one-dimensional recompression stiffness calculated through $p$ and $\lambda$. As a result, the expression of $F_{consol}$ will return values close to $G_{c,min}$ if the loading is within the dilatancy surface ($M^{cur} \ll M^d$) or close to $G$ if the loading is near the dilatancy surface ($M^{cur} \approx M^d$) (Boulanger et al. (2018)).

Furthermore, to perform stability analyses after strong earthquakes and to account for the reduction of soil undrained resistance (for its rate dependency or also in case of degradation or remolding phenomena), it is possible to reduce the undrained strength by using a reduction coefficient $F_{Su}$, which is a further parameter of the model. This parameter does not act directly on $S_u$ but it shifts the CSL

$$e_{cs} = \Gamma - \lambda \cdot ln\left[\frac{p}{F_{Su} \cdot (1kPa)}\right] \qquad \textit{Eq. 56}$$

Further details regarding the use of the parameters $F_{consol}$ and $F_{Su}$ for post-shaking analyses, i.e. when the flag $Post - shake$ is selected equal to 1, will be given in the next section.

# 3. Model parameters and state variables

PM4Silt is implemented for PLAXIS 2D as a User Defined Soil Model (UDSM). In this section, a detailed description of the model parameters and state variables is presented.

## 3.1. Model Parameters

The input parameters of PM4Silt can be grouped into three categories: primary, secondary, and optional:

- Primary input parameters: $S_u$ (or $S_{u,ratio}$), $G_0$ , $h_{p0}$
- Secondary input parameters: $n^G$, $h_0$, $e_0$, $\lambda, \phi_{cv}, n^{b,wet}, n^{b,dry}, n^d, A_{do}, r_{u,max}, z_{max}, c_z, C_\varepsilon, C_{GD}, C_{Kaf}, \nu$
- Optional input parameters
  - Post-shake reconsolidation: $Post\ Shake$, $F_{Su}$ and $CG_{consol}$
  - Alternative definition of $S_u$ : $\Psi_R$, $d_R$ and $\phi_c$, $c_c$

To simplify the calibration process and give the order of magnitude of the secondary parameters, reference values have provided in Boulanger et al. (2018) which can be used as a first-tentative during the process or retained in case the required experimental data are not available. If a zero value is assigned in the PLAXIS 2D Input user interface, the reference values proposed in Boulanger et al. (2018) will be automatically used internally.

While primary and secondary parameters are used in every kind of analysis, the two optional parameters $F_{Su}$ and $CG_{consol}$ are used only when $Post\ shake$ is equal to 1. Furthermore, as explained in Section 2.7, the last four parameters can be used to consider the variability of $S_u$ in numerical analyses where $K_0$ is not constant.

The entire set of parameters is depicted in Figure 10. All the parameters and state variables are initialized based on the effective stress state at the beginning of the first calculation phase in which PM4Silt is employed. If the model is used in different phases of a given analysis, by default the initialization is performed only at the first phase in which PM4Silt is used therefore, if a reinitialization of the state variables (and the computation of $S_u$) is required, the user can select the option *Reset state variables* in the Phases window of the PLAXIS Input program.

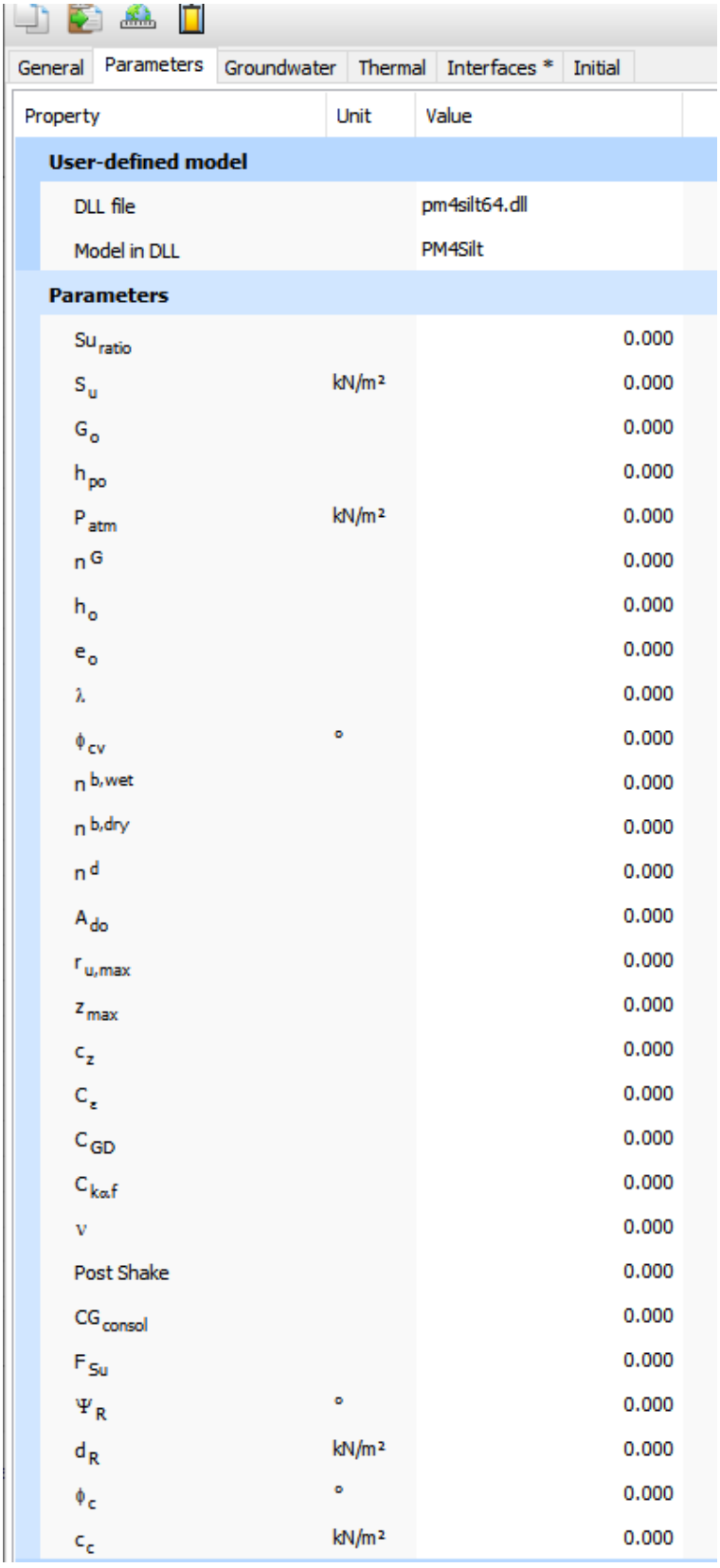


Figure 10. *Parameters of the User Defined Soil Model (UDSM) in the Material data set window.*

### 1.1.6 Primary parameters

**· $S_u$ (or $S_{u,ratio}$): Undrained strength at critical state (or undrained strength ratio).**

The parameter $S_u$ is used to determine the position of the CSL in the compressibility plane (as shown in Figure 3). $S_u$ can be entered by the user or can be initialized based on the value of the undrained strength ratio $S_{u,ratio}$. Only one parameter, that is either $S_u$ or $S_{u,ratio}$, should be specified by the user and in case both values are different than zero, only $S_u$ will be used.

When $S_{u,ratio}$ is assigned as an input, $S_u$ is then computed from the vertical effective stress at the beginning of the first phase of a given analysis in which PM4Silt is used. If the model is used in different phases, the vertical effective stress considered in the computation of $S_u$ can be reset, as already mentioned, by selecting *Reset state variables* in the Phases window of the PLAXIS Input program**.** To select the appropriate value for $S_u$ (or the equivalent $S_{u,ratio}$), the user must consider, as clarified in Boulanger et al. (2018), that

- Although silts and clays can exhibit a peak undrained shear strength, the value of $S_u$ at critical state should be estimated to assign the input parameter.

- The undrained strength is intrinsically characterized by a rate dependency (e.g. Sheehan et al. (1997)). Due to the high rate of loading happening during seismic events, an increase of $S_u$ should be considered for dynamic analyses. For this reason, as laboratory experiments are commonly performed by applying the loading through slower processes, the calibrated value of $S_u$ needs to be increased about 20-40% to make it coherent with earthquake loadings (Boulanger et al. (2007)).

The undrained strength $S_u$ can be determined through different methods:

- Laboratory tests, e.g. consolidated undrained triaxial test or DSS tests
- In situ tests, typically cone penetration or vane shear tests
- Empirical correlations between the undrained strength ratio and OCR.

In boundary values problems where the effective stress is not homogeneous, the choice of initializing $S_u$ by using $S_{u,ratio}$ allows one to consider a dependency of $S_u$ on the confinement, which is valid for homogeneous values of OCR and $K_0$ (and homogeneous effective stress path). Also, the variability of $S_u$ in the domain can be considered by defining multiple layers. In some cases, as for the analysis of embankments, more complex distributions of the undrained strength resulting from different consolidation stress states can be considered using the method described in Section 2.1.

**· $G_0$: Initial shear modulus coefficient.**

$G_0$ controls the small strain shear modulus in Eq. 37 which, at the state initialization, is

$$G = G_0 \cdot p_{atm} \cdot \left[\frac{p}{p_{atm}}\right]^{n_G} CSR \qquad \textit{Eq. 57}$$

The shear modulus coefficient $G_0$ is a constant dimensionless parameter that can be assessed by knowing the small strain shear modulus at a reference mean effective stress. The elastic shear modulus should be calibrated to fit estimated or measured shear wave velocities $V_s$ according to

$$G = \rho(V_s)^2 \qquad \textit{Eq. 58}$$

where $\rho$ is the saturated density. Two approaches to determine $G_0$ are reported in Boulanger et al. (2019b).

· **$h_{p0}$: Contraction rate parameter**

This parameter has an influence on the dilatancy $D$ in the case of contracting behavior (see Eq. 51). The higher the value assigned to $h_{p0}$, the lower the corresponding value of $D$. For this reason and the effect on the rate of reduction of $p$ in undrained conditions, $h_{p0}$ has a strong influence on the number of cycles required to trigger the cyclic resistance. This parameter has no direct physical meaning and therefore its evaluation requires an iterative procedure. The user should tweak the value of $h_{p0}$ until it is possible to match the cyclic strength curves representing the relationship between the Cyclic Resistance Ratio (CRR) and the number of uniform loading cycles required to cause a 3% shear strain (or any other preferred criterion) under undrained cyclic loading conditions. Examples of $h_{p0}$ calibration are reported in Boulanger et al. (2019a).

The link existing among the cyclic resistance, the undrained strength, and the OCR, valid in the silts and clays exhibiting a stress-history normalized behavior, allows estimating the CRR of these soil deposits through three different approaches (Boulanger et al. (2007)).

(1) *CRR evaluation from cyclic laboratory testing.*

(2) *CRR evaluation from a measured $S_u$ profile.* When a direct evaluation through experimental laboratory tests is not available, empirical relationships have been proposed to provide a reference value of CRR for earthquakes of magnitude equal to 7.5, i.e. $CRR_{M=7.5}$ , for instance, the empirical relationship

$$CRR_{M=7.5} = C_{2D} \cdot \left[\left(\frac{\tau_{cyc}}{S_u}\right)_{N=30}\right] \cdot \frac{S_u}{\sigma'_{vc}} \cdot K_\alpha \qquad \text{Eq. 59}$$

$C_{2D}$ is a correction factor for two-dimensional versus one-dimensional cyclic loading, usually assumed as 0.96. $K_\alpha$ is the static shear stress ratio correction factor to approximate the effect of initial static shear stresses, $\left(\frac{\tau_{cyc}}{S_u}\right)_{N=30}$ is the ratio of cyclic stress $\tau_{cyc}$ to monotonic undrained resistance $S_u$ required to trigger the peak shear strain of 3% with 30 uniform cycles of loading. Despite many other factors (e.g. aging or OCR) influence its value, it is suggested that $\left(\frac{\tau_{cyc}}{S_u}\right)_{N=30}$ is assumed equal to 0.83 with a variation of ±15% for natural clay-like soils subjected to DSS loading conditions (Boulanger et al. (2004) and Boulanger et al. (2007)). After replacing the values for the coefficients $C_{2D}$ and $\left(\frac{\tau_{cyc}}{S_u}\right)_{N=30}$, the $CRR_{M=7.5}$ for fine-grained soils can be expressed as

$$CRR_{M=7.5} = 0.8 \cdot \left(\frac{S_u}{\sigma'_{vc}}\right) \cdot K_\alpha \qquad \text{Eq. 60}$$

The scaling to earthquakes of magnitude different than 7.5 can be finally done through $CRR(M) = MSF(M) \cdot CRR_{M=7.5}$ , where MSF is a magnitude scaling factor that can be determined from Figure *11*.

(3) *CRR evaluation from a consolidation stress history profile*

By combining the previous equation with the classic relationship that links the normalized monotonic undrained resistance with the OCR, the $CRR_{M=7.5}$ can also be estimated through

$$CRR_{M=7.5} = 0.8 \cdot S \cdot OCR^m \cdot K_\alpha \qquad \text{Eq. 61}$$

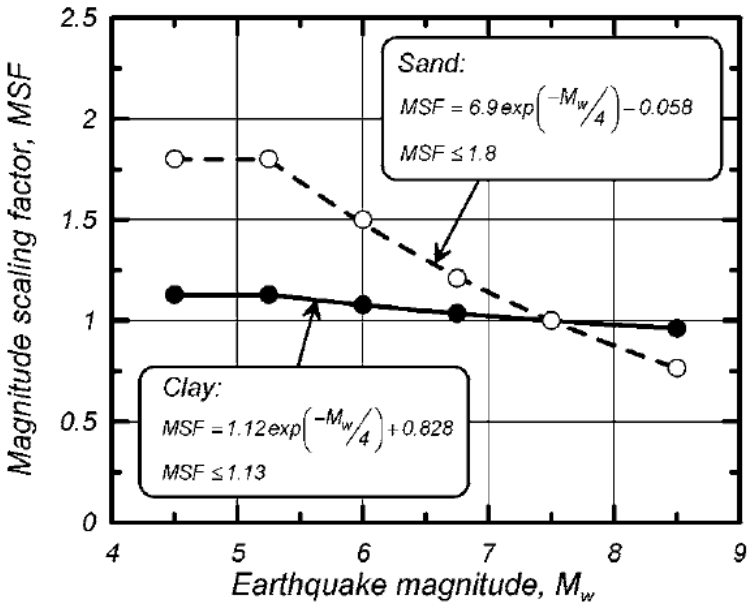


Figure 11. *Magnitude Scaling Factor (MSF) as a function of the earthquake magnitude M.*

$S$ and *m* being coefficients to be estimated empirically. As also recalled in Boulanger et al. (2004) for homogenous, low-plasticity, high-plasticity, and sedimentary clays, Ladd (1991) proposed 0.22 and 0.8 for $S$ and *m*, respectively. With these assumptions, Eq. 61 can be rewritten as

$$CRR_{M=7.5} = 0.18 \cdot OCR^{0.8} \cdot K_{\alpha} \qquad \text{Eq. 62}$$

### 1.1.7 Secondary parameters

**· $p^{atm}$: atmospheric pressure (default value $101.3\ kPa$)**

It represents the atmospheric pressure in the unit set being used for the analysis. When set to zero the value of 101.3 is selected by default. If a unit system different from kPa is used, the correct value must be explicitly provided in input.

**· $n^G$: Shear modulus exponent (default value $0.75$)**

$n^G$ controls how the shear modulus varies with the confining stress. This parameter can be determined together with $G_0$ to fit the values of $V_s$ or $G$.

**· $h_0$: Plastic modulus ratio (default value $0.5$)**

This parameter is used to increase or reduce the hardening modulus $K_P$ (see Eq. 42). The effect of $h_0$ on the predicted mechanical behavior can be easily understood by examining the equations of the stiffness matrix (Eq. 11) according to which increasing values of $K_p$ bring the elastic-plastic stiffness closer to the elastic one. Therefore, higher values of $K_p$ reduce the degradation of the elastic stiffness with the development of plastic strains. For this reason, $h_o$ influences (i) the stiffness on the shear level which modifies the trend of monotonic stress-strain behavior, (ii) the shape of the shear modulus degradation curve, and (iii) the damping ratio curve. Furthermore, increasing values of $h_o$ tend to move the shear modulus reduction curve towards the right part of the plot, consistently with what is observed for materials with increasing PI. The parameter $h_o$ can be used to adjust the dependency of the secant shear modulus and damping ratio on the shear strain level (Boulanger et al. (2019a)). In

Boulanger et al. (2019b) it is suggested to calibrate this parameter against either monotonic or cyclic tests, in accord with the specific case at hand.

· $e_0$: **Initial void ratio (default value $0.9$).**

Initial void ratio of a soil layer.

· $\lambda$: **Slope of the CSL (default value $0.6$).**

The slope of the critical state line in ln(p)-e space.

· $\phi_{cv}$: **Friction angle at CS (default value $32^\circ$).**

· $n^{b,wet}$: **Bounding surface parameter (default value $0.8$).**

This parameter influences the peak value of the undrained resistance $S_u$ and it should be chosen to match the trend of behavior observed in monotonic undrained shear tests. The upper and lower limits are 1.0 and 0.1, respectively.

· $n^{b,dry}$: **Bounding surface parameter (default value $0.5$).**

This parameter influences peak friction angles for states denser than CS and modifies the shape of the BS on the dry side (Figure *8*). Due to the constraint of no-intersection between the current state and the BS, the shape of the bounding in the dry side influences the trend of the effective stress path for states denser than CS.

· $n^d$: **Dilatancy surface parameter (default value $0.3$).**

This parameter influences the transition between contractive and dilative mechanical response.

· $A_{do}$: **Dilatancy parameter (default value $0.8$).**

This parameter affects the dilatancy $D$.

· $r_{u,max}$: **Maximum excess pore pressure ratio (default value 0).**

$$r_{u,max} = \frac{\Delta p}{p_o} \qquad \textit{Eq. 63}$$

$\Delta p$, $p_o$ being the maximum possible reduction and the initial mean effective stresses, respectively. $r_{u,max}$ affects the value of $p_{min}$ which is an important reference value of the mean effective stress appearing in several equations of the model (see for instance Eq. 49). In PM4Silt, the maximum

reduction of $p$ during undrained cyclic loadings is predefined and, if desired, it can be regulated through the parameter $r_{u,max}$. $p_{min}$ is computed internally and it is based on the initial effective stress and $S_{u,ratio}$ when the 0 value is assigned to $r_{u,max}$, that is

$$p_{min} = \frac{p_{cs}}{8} = \frac{1}{4}\left(\frac{S_u}{M}\right) \qquad \text{Eq. 64}$$

or it is computed explicitly according to the value of $r_{u,max}$ when explicitly assigned as an input, i.e.

$$p_{min} = \left(1 - r_{u,max}\right)\frac{p_o}{2} \qquad \text{Eq. 65}$$

The value $2\,p_{min}$ represents the minimum mean effective stress reachable during undrained cyclic loadings. To estimate $r_{u,max}$ it is important to account for the different definition of $r_u$ with respect to the classical one used to interpret laboratory test results. For instance, for direct simple shear tests $r_u = \frac{\Delta u}{\sigma_{vo}} = \frac{\sigma_{v0} - \sigma_v}{\sigma_{vo}}$. It is worth noting that in the numerical simulation of simple shear tests the $r_{u,max}$ coincides with $\frac{\sigma_{v0} - \sigma_v}{p_o} = \frac{\Delta u}{p_o}$.

**· $z_{max}$: Maximum value of fabric tensor (default value $0.0$)**

This parameter determines the maximum value of the fabric tensor $z_{ij}$. If the input value is equal to 0, this parameter is automatically computed based on the value of the $S_{u,ratio}$, i.e.

$$\begin{aligned} z_{max} &= 10 && for\ S_{u,ratio} \le 0.25, \\ z_{max} &= 40\,S_{u,ratio} && for\ 0.25 < S_{u,ratio} \le 0.50, \\ z_{max} &= 20 && for\ S_{u,ratio} > 0.50\,. \end{aligned} \qquad \text{Eq. 66}$$

$z_{max}$ starts influencing the evolution of the dilatancy fabric tensor only after that $z_{cum}$ reaches the value $2\,z_{max}$. Higher values of $z_{max}$ tend to increase the maximum value of the excess pore pressure while reducing the width of the hysteresis loop and the cyclic strength, steepen the CRR-cycles curve, and increase the rate of strain accumulation.

**· $C_z$: Fabric growth parameter (default value $100$).**

This parameter controls the evolution of the fabric dilatancy tensor $z_{ij}$ and has a strong influence on the CRR curves. As shown in Eq. 36, a reduction of $C_z$ results into a decrease in the growth rate of the fabric-dilatancy tensor and the corresponding $z_{cum}$. The fabric tensor remains equal to zero until the stress state reaches the DS. As a consequence, $C_z$ will not influence the response before the stress state reaches the DS. In the case of dilatant behavior, when it is necessary to reduce the level of cumulated strains, it is preferable to modify $C_z$ rather than varying $h_{p0}$. This parameter can also be used to adjust some portions of the effective stress path and the stress-strain relation.

**· $C_\varepsilon$: Strain accumulation parameter (default value $0$).**

This plays a role in D for the case of dilating behavior, appearing at the denominator of $A_d$ (see equation A1. 3). When this parameter is prescribed equal to 0, the default value is computed internally as

$$C_\varepsilon = 0.5 + 1.2\langle S_{u,ratio} - 0.25\rangle \leq 1.3 \qquad \text{Eq. 67}$$

Analogously to the role of $C_z$, the parameter $C_\varepsilon$ has an influence on the mechanical behavior predicted by the model only after that the stress state reaches the DS. Specifically, it reduces the tendency to dilate for stress paths with a negative increment of mean stress and decreases the stiffness of the material, hence enabling faster development of strains.

**· $C_{GD}$: Degradation factor (default value 3).**

$C_{GD}$ affects the degradation of the shear modulus $G$ when $z_{cum}$ becomes larger than $z_{max}$. Consequently, this parameter influences the response when the amount of shear strain is very large and allows to account for the stress-strain behavior of liquefied soils as the maximum degradation reaches a factor of $1/C_{GD}$ (see Boulanger et al. (2018)).

**· $C_{Kaf}$: Plastic modulus factor (default value 4).**

As remarked by Boulanger et al. (2018), $C_{Kaf}$ can adjust the effect that the initial static shear stress has on plastic modulus and hence on cyclic strength. The effect of this parameter is small for states looser than CS and becomes more important for states denser than CS.

**· $\upsilon$: Poisson's ratio (default value 0.3)**

In the case of one-dimensional consolidation, as the model is not able to predict plastic behavior, $K_0$ can be computed using the elastic relation $K_0 = \nu/(1-\nu)$.

### 1.1.8 Post-shaking analysis parameters

**· $Post\ shake$: Post-shake reconsolidation flag (default value 0)**
**· $F_{Su}$: Post-shake strength reduction coefficient (default value 1.0)**
**· $GC_{consol}$: post-shake shear modulus degradation parameter (default value 2.0)**

The user can use the $Post\ shake$ flag to perform post-shake reconsolidation analyses by assigning to it a value equal to 1 (this option is inactive if $Post\ shake = 0$). In the case of $Post\ shake = 1$ a reduction of stiffness and resistance is performed according to the equations presented in 2.7. In this case, two additional parameters must be specified in the input, $F_{Su}$ and $GC_{consol}$. These parameters allow the user to model a reduction of the undrained resistance and/or the stiffness which is sometimes found in practice. The user should create a copy of the material and assign the value 1 to $Post\ shake$ and the estimated values for $F_{Su}$ and $GC_{consol}$.

### 1.1.9 Alternative definition of a variable Undrained Shear Strength

**· $\phi_c, c_c, \psi_R, d_R$: parameters to estimate $S_u$ in presence of different consolidation conditions from results of isotropically consolidated undrained triaxial tests**

These parameters are aimed to prescribe the undrained strength variable with the consolidated stress state. This method is an alternative to prescribing either $S_u$ or $S_{u,ratio}$ and is automatically activated when both $\phi_c$ and $\psi_R$ are different than zero, regardless of the value of $S_u$ or $S_{u,ratio}$. In this manner, the method proposed by Montgomery et. al (2014), applied also to PM4Silt by Boulanger (2019), described in Section 2.1 is considered to account for a variable $S_u$ in presence of different conditions of consolidation in the domain.

## 3.2. State variables

In PLAXIS Output the user can plot a list of variables related to the model (Figure *12*). The list includes the state variables and additional variables are included to facilitate the interpretation of results. In addition, also parameters depending on the initial effective stress, i.e. the small strain bulk and shear moduli, are provided in the list of state variables. Here follows a description of these variables.

· $\boldsymbol{S_{u,ratio}}$: Undrained strength ratio.

· $\boldsymbol{S_u}$: Undrained strength.

· $\boldsymbol{r_{u,max}}$: Maximum excess pore pressure ratio, as provided in input.

· $\boldsymbol{p_{min}}$: $2\ p_{min}$ represents the minimum value of the current mean effective stress, i.e. the following restriction must be satisfied $p_{cur} \geq 2 \cdot p_{min}$. It can be estimated based on $r_{u,max}$ or $p_{cs}$. For additional details see Section 2.6.

· $\boldsymbol{z_{max}}$**:** Parameter influencing the maximum value of the fabric-dilatancy tensor.

· $\boldsymbol{C_\varepsilon}$ : Strain accumulation parameter.

· $\boldsymbol{M}$ **:** Critical state stress ratio.

· $\boldsymbol{\Gamma}$ **:** Void ratio corresponding to 1 kPa on the CSL.

· $\boldsymbol{p_{cs}}$**:** Mean effective stress at the critical state.

· $\boldsymbol{\xi}$ **:** State parameter.

· $\boldsymbol{e}$**:** Current void ratio

· $\boldsymbol{M_{cur}}$**:** Current value of the stress ratio.

· $\boldsymbol{K}$**:** current bulk modulus.

· $\boldsymbol{G}$**:** current shear modulus

· $\boldsymbol{\alpha_{static} = \frac{\tau_{xy,0}}{\sigma_{v,0}}}$**:** The static shear stress ratio is the ratio between the initial shear stress and the initial vertical effective stress. $\alpha_{static}$is shown in output as a value different than zero in case of a customized distribution of the undrained resistance which is provided by using the parameters $\boldsymbol{\phi_c, c_c, \psi_R}$ and $\boldsymbol{d_R}$. These parameters have an influence on the undrained resistance. As recalled by Eq. 59, the undrained cyclic resistance depends on $\alpha_{static}$, therefore plotting this variable before the dynamic calculation can be useful to better calibrate the cyclic resistance.

· $\boldsymbol{K_c}$ and $\boldsymbol{K_0}$**:** Ratios between the initial principal effective stresses and the initial effective stress, i.e. $K_c = \sigma_1\ /\sigma_2$ and $K_0 = \sigma_h\ /\sigma_v$, respectively. Analogously to $a_{static}$, $K_c$ and $K_0$ are characterized by non-zero values when the undrained resistance is distributed according to the trend prescribed through the parameters $\boldsymbol{\phi_c, c_c, \psi_R}$ and $\boldsymbol{d_R}$. They influence the computation of $S_u$ according to Eq. 24.

· $\boldsymbol{\sigma_{v,0}}$ **:** Initial vertical effective stress.

· $\boldsymbol{r_u}$: Current value of the ratio $\boldsymbol{\frac{p_0 - p}{p_0}}$ . The sign of $\boldsymbol{r_u}$ indicates a dilative or contractive response. In undrained DSS tests, the numerator coincides with $\Delta u$ when the condition $\Delta\sigma_h = \Delta\sigma_v = \Delta u$ is reached.

· $\boldsymbol{r_{u,Extreme}}$**:** Maximum value attained by $r_u$ during a prescribed loading history. The maximum value this variable can reach is $\boldsymbol{r_{u,Limit}}$.

· $\boldsymbol{\gamma/2_{MaxExtreme}} = \sqrt{\left(\frac{\varepsilon_{xx}+\varepsilon_{yy}}{2}\right)^2 + \boldsymbol{\varepsilon_{xy}^2}}$ : Maximum value of the Mohr's circle radius in the strain space.

· $\boldsymbol{BCI}$ **(Bounding Correction Indicator)**: Integer which can be either 0 or 1. In the case of a unity value, BCI indicates a violation of the BS according to the prescribed value of $K_0$. In this case, the initial stress is internally reinitialized to satisfies a consistent prescription of the bounding.

· $\boldsymbol{\gamma/2_{Max}} = \sqrt{\left(\frac{\varepsilon_{xx}+\varepsilon_{yy}}{2}\right)^2 + \boldsymbol{\varepsilon_{xy}^2}}$**:** Current value of the Mohr's circle radius in the strain space.

· $\boldsymbol{M_d}$: Dilatancy surface (DS) stress ratio.

· $\boldsymbol{M_b}$**:** Bounding surface (BS) stress ratio.

· $\boldsymbol{D}$**:** Dilatancy.

· $\boldsymbol{\alpha_{xx}}$**:** Component $xx$ of the back-stress ratio tensor.

· $\boldsymbol{\alpha_{yy}}$**:** Component $yy$ of the back-stress ratio tensor.

· $\boldsymbol{\alpha_{xy}}$**:** Component $xy$ of the back-stress ratio tensor.

· $\boldsymbol{r_{u,Limit} = (p_o - 2p_{min})/p_o}$**:** Value of $r_u$ calculated with the minimum value of the mean effective stress. $r_{u,Limit}$ is defined equal to $r_{u,max}$ when $r_{u,max}$ is given as an input to control the value of $p_{min}$ otherwise, it is the value computed according to Eq. 64. While in sands this limit value is usually equal to 1, in silts generally can range between 0.~~6~~8 and 1.

· $\boldsymbol{Ipr = r_{u,extreme}/r_{u,Limit}}$**:** Indicator for the reduction of the mean effective stress. For contracting behavior, the range of values for $Ipr$ is limited between 0 and 1. In the case of dilating behavior, $Ipr$ can be negative and indicates the distance with respect to $\boldsymbol{r_{u,Limit}}$.

· $\boldsymbol{\tau_{xy,ratio} = \tau_{xy}/\sigma_{v0}}$**:** Normalized value of the shear stress with respect to the initial vertical effective stress.

· $\boldsymbol{\tau_{xy,ratio,Extreme}}$**:** Maximum value of $\tau_{xy,ratio}$ during the loading history.

It is worth noting that many other variables are exposed in the user interface, although these will not be described in this section as they are used for the numerical integration of the model.

All the parameters of PM4Silt included between the output state variables and $\sigma_{v0}, \alpha_{static}$. $K_o$ $K_c$ and BCI all remain constant after the initialization. The distributions of $\alpha_{static}$, $K_o$ and $K_c$ are useful for checking the values of $S_u$ automatically computed based on the initial vertical effective stress and initial $K_o$ through the four optional parameters. For this reason, these are shown only in this particular case. All the other quantities are updated at each step of the calculation.

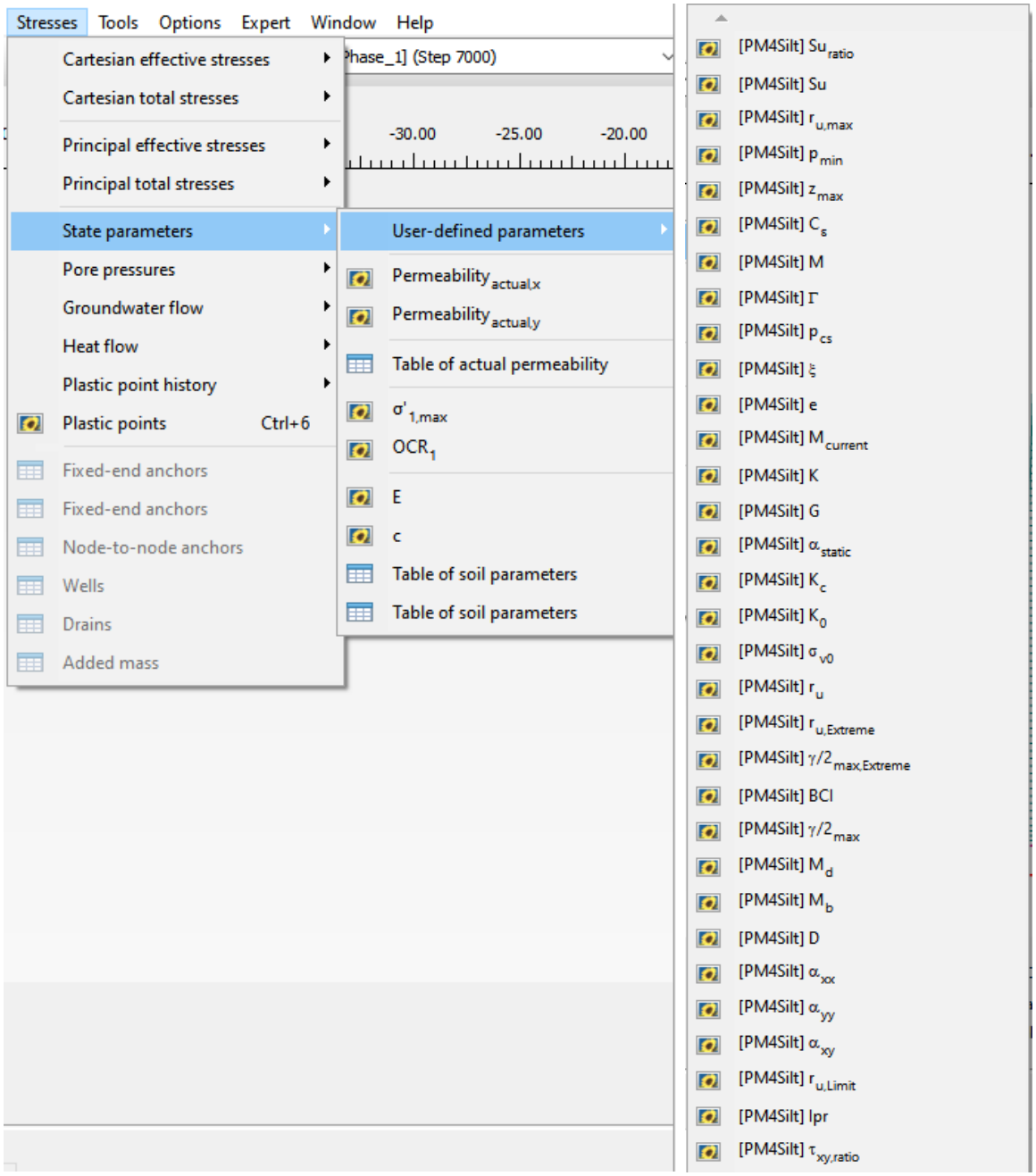


Figure 12. *State variables of PM4Silt.*

# 4. Model response in undrained monotonic and cyclic loading conditions

To demonstrate the performance of the model, three monotonic undrained DSS tests have been solved through the PLAXIS SoilTest facility by using the calibrations proposed in Boulanger et al. (2018) and reported in Table 1. For monotonic tests, the main difference in the three calibrations consists of the different values of $S_{u,ratio}$.

*Table 1. Summary of the calibrations. Secondary parameters are set to zero, therefore at their default values.*

| **PRIMARY PARAMETERS** | **Calibration** | | | **Units** |
|---|---|---|---|---|
| | ***A*** | ***B*** | ***C*** | |
| $S_{u,ratio}$ | 0.25 | 0.5 | 0.75 | |
| $G_0$ | 588 | 776 | 913 | |
| $h_{po}$ | 20 | 50 | 60 | |
| | | | | |
| **SECONDARY PARAMETERS** | **Calibration (Default values)** | | | **Units** |
| $p_{atm}$ | 101.3 | | | [ kPa ] |
| $n_G$ | 0.75 | | | |
| $h_0$ | 0.5 | | | |
| $e_0$ | 0.9 | | | |
| $\lambda$ | 0.06 | | | |
| $\varphi_{cv}$ | 32 | | | [ ° ] |
| $n^{b,wet}$ | 0.8 | | | |
| $n^{b,dry}$ | 0.5 | | | |
| $n^d$ | 0.3 | | | |
| $A_{do}$ | 0.8 | | | |
| $r_{u,max}$ | 0 ( $p_{min} = p_{cs}/8$) | | | |
| $z_{max}$ | $10 \leq 40(S_u/\sigma'_{vc}) \leq 20$ | | | |
| $C_z$ | 100 | | | |
| $C_\varepsilon$ | $0.5 \leq (1.5S_u/\sigma'_{vc} + 0.2) \leq 1.3$ | | | |
| $C_{GD}$ | 3.0 | | | |
| $C_{kaf}$ | 4.0 | | | |
| $\upsilon$ | 0.3 | | | |
| | | | | |
| **PARAMETERS FOR POST-SHAKING AND ALTERNATIVE DEFINITION OF $S_u$** | **Calibration (Default values)** | | | **Units** |
| Post Shake | 0 | | | |
| $CG_{consol}$ | Not used when Post Shake = 0 | | | |
| $F_{Su}$ | 1.0 | | | |
| $\Psi_R$ | Not used when 0 ($S_u$ or $S_{u,ratio}$ is specified) | | | [ ° ] |
| $d_R$ | Not used when 0 ($S_u$ or $S_{u,ratio}$ is specified) | | | [ kPa ] |
| $\phi_c$ | Not used when 0 ($S_u$ or $S_{u,ratio}$ is specified) | | | [ ° ] |
| $d_c$ | Not used when 0 ($S_u$ or $S_{u,ratio}$ is specified) | | | [ kPa ] |

Figure 13 shows results obtained in three simulations of strain-controlled undrained DSS tests performed with the same initial vertical effective stress while $\sigma'_{y0}$ and $K_0$ assuming values in correspondence to the three calibrations in Table 1. Specifically, it is shown that increasing values of $S_{u,ratio}$ determine an increase of the undrained strength (i.e. higher values of $S_u$) therefore the position of the BS tends to move in the upper part of the stress space (Figure 13 (b)). As shown in Figure 13 (b), different $S_u$ result to three different values of $p_{cs}$, corresponding to the intersection

between BS and CSL, consistently with the stress path direction. In the analytical framework of the model $\Gamma$ is defined as a function of $p_{cs}$ and, due to this reason, differences in $\Gamma$ cause three initial state parameters for the same initial effective stress state. The different positions of the CSL corresponding to the calibrations A, B, and C can be observed in Figure 13 (a) showing the undrained stress path and the resulting mean effective stress at the critical state. The contracting and dilating characteristics of the undrained DSS stress path can be observed in Figure 13 (b,d).

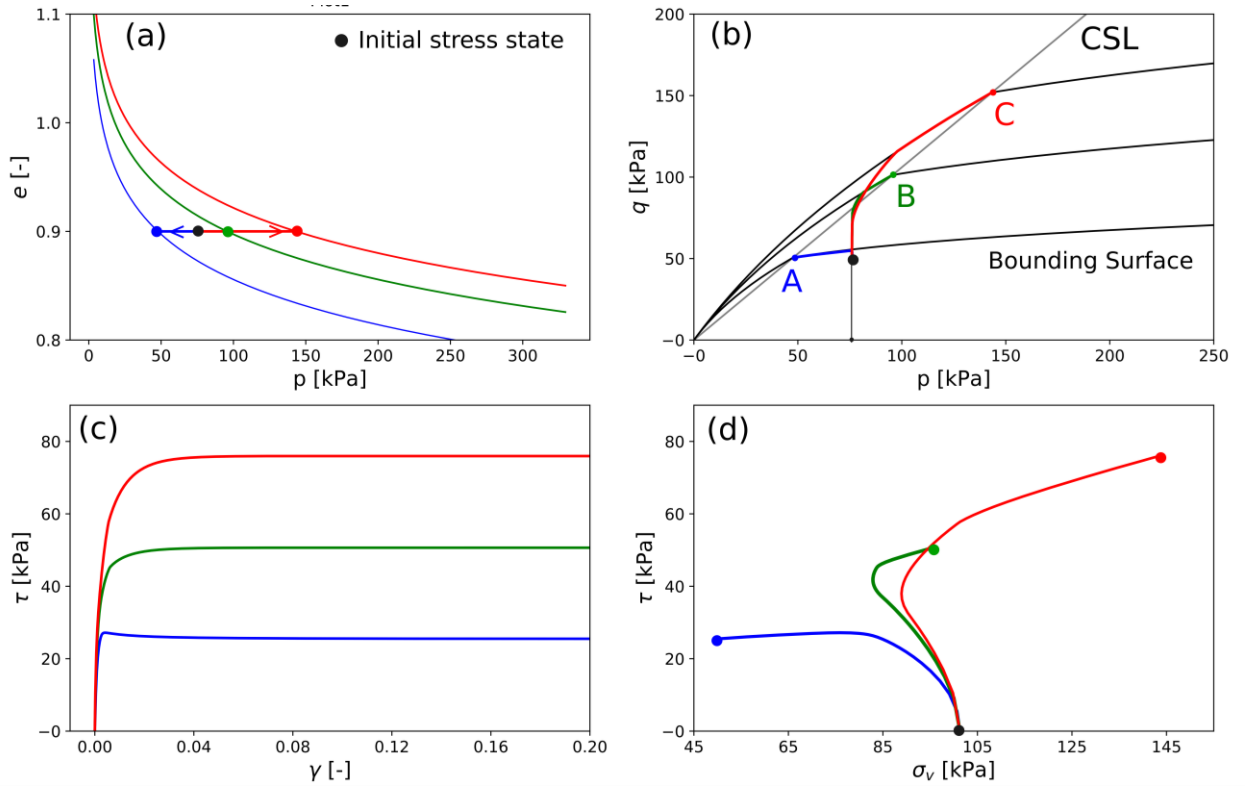


Figure 13*: Monotonic undrained DSS performed with the parameters A, B, and C. The same initial effective stress $\sigma'_{vc}$ =101.3 kPa and K0 = 0.5 apply. The red, green, and blue lines correspond to the results obtained with the sets of parameters C, B, and A, respectively.*

## 4.1. Simulations of stress-controlled CDSS tests and CRR vs N curves

A series of undrained Cyclic Direct Simple Shear (CDSS) tests have been performed by using the parameters reported in Table 1 and by loading the sample with a given increment of shear stress (i.e. a given Cyclic Stress Ratio (CSR) defined as $\Delta\tau_{xy}/\sigma'_{v0}$). In Figure *14* and Figure *15*, the stress-strain behavior resulting from cyclic undrained DSS is shown to emphasize the evolution of different cyclic responses obtained by selecting the calibrations A and C of Table 1. Although the two tests are performed with the same $\sigma'_{y0}$ and $K_0$, they are loaded with different shear stress increments, therefore having different CSR corresponding to CSR=0.175 ($\Delta\tau_{xy} = 17.73$) and CSR=0.70 ($\Delta\tau_{xy} = 70.91$) for the calibration A and C, respectively. Form Figure *14* it is possible to observe as the soil response is characterized by an initial contracting behavior and it needs many cycles to reach the cyclic mobility. To better visualize the cycles which cumulate a shear strain larger than 3%, the stress-strain behavior has been plotted with two different colors, green and orange, denoting cycles with shear strain smaller and larger than 3%, respectively. A different scenario is depicted in Figure *15* where the stress path starts dilating from the beginning of the loading although showing an overall reduction of the mean effective stress. Although the two stress paths are characterized by a different loading (i.e. different $\Delta\tau_{xy}/S_{u,ratio}$), they show the ability of the model to simulate two opposite trends of constitutive behavior and their different effect on triggering mechanisms of cyclic mobility. It is worth noting that

the two stress paths are also characterized by two different values of the minimum mean effective stress which is explained by the dependency of $S_u$ on $p_{min}$ as reported in Eq. 64.

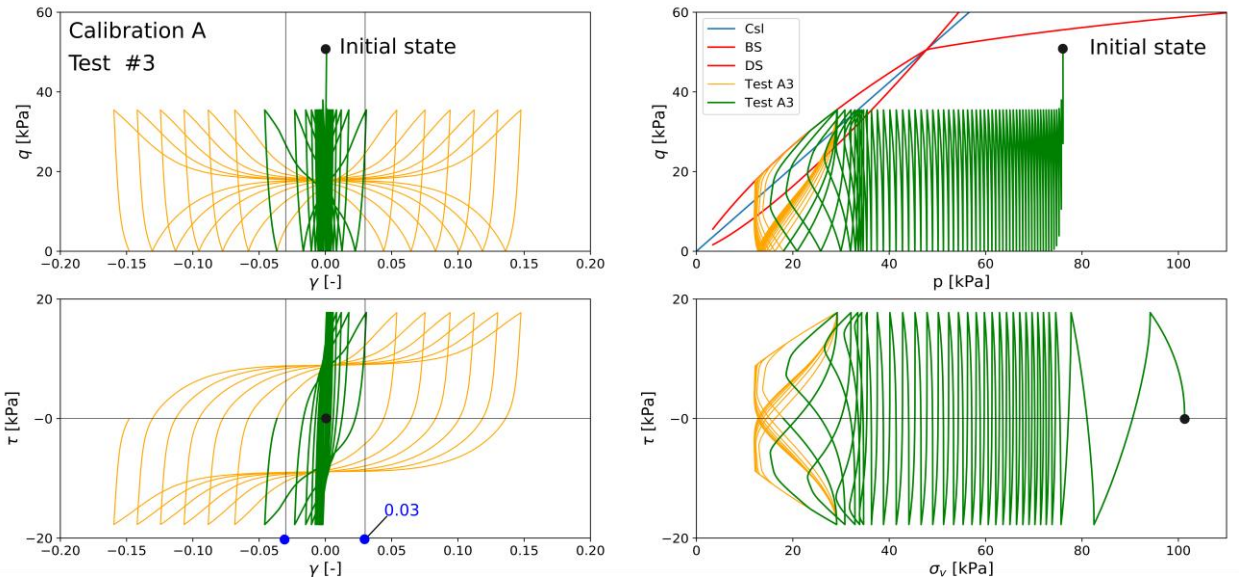


Figure 14*: Undrained cyclic DSS test performed for normally consolidated silt, calibration A. In this test, the increment of shear stress is equal to* $\Delta\tau_{xy} = 17.73\ kPa$.

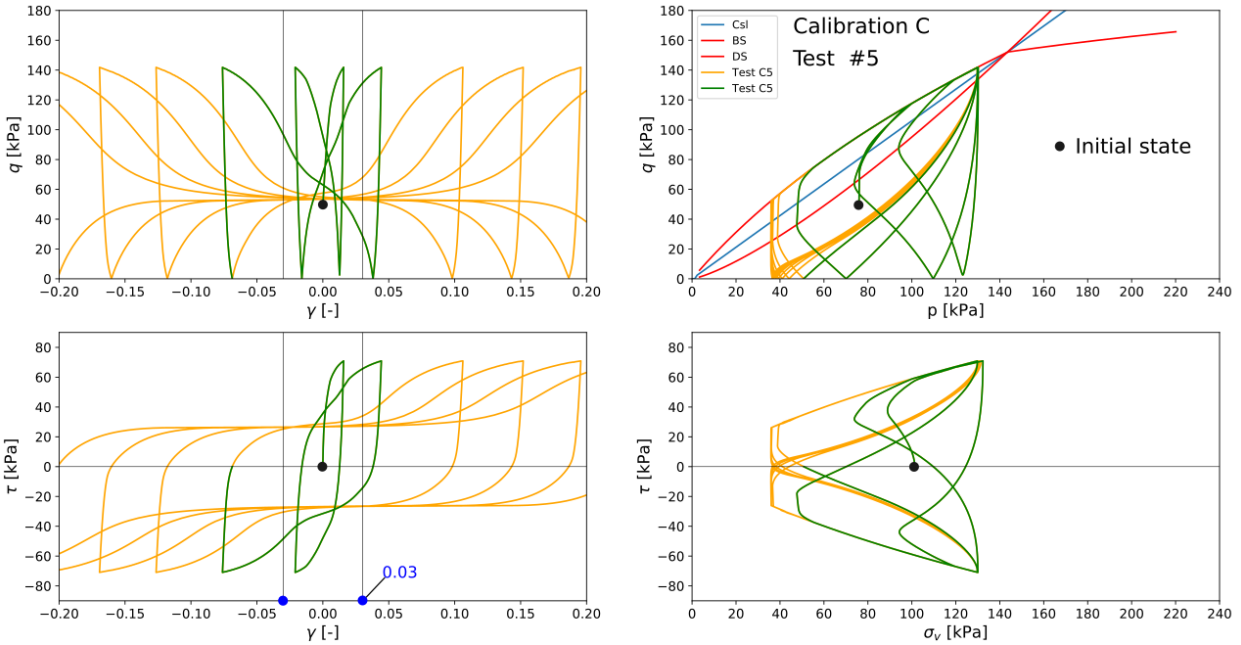


Figure 15*: Undrained cyclic DSS test performed for normally consolidated silt, calibration C. In this test, the increment of shear stress is equal to* $\tau_{xy} = 70.91\ kPa$.

In soil dynamics, it is common practice to characterize the cyclic resistance of soils by relating the CSR with the number of cycles required to reach a given value of total shear strain. These curves, generally referred to as CSR-N curves, are plotted in Figure *16* for the three calibrations reported in Table 1, considering a single amplitude maximum shear strain of 3%. To verify the proposed implementation of PM4Silt, the results for the three calibrated parameters are also compared with the plots reported in Boulanger et al. (2018), showing a good agreement between the two implementations of the model. Further details about this plot are given in

Table 2 in which the entire set of initial conditions are presented along with the corresponding values of the number of cycles employed for each undrained CDSS to reach $\gamma_{xy} = 3\%$ . From Figure 16 it is possible to notice that for the case N=1 the CSR tends to be equal to the prescribed value of $S_{u,ratio}$. However, for the calibration A and N=1, the CSR tends to be slightly higher than the monotonic undrained resistance at CS which is explained by the fact that the initial assumption of $n_{b,wet} = 0.8$ allows reaching a peak resistance slightly higher than 0.25 (see Figure 13). The trend of the CSR curves is mainly influenced by the parameters $h_{po}$, $C_\varepsilon$, $z_{max}$, and $C_z$.

As remarked in Section 3.1, $h_{po}$ and $C_\varepsilon$ modify the rate of the volumetric plastic strain for contracting and dilating behavior, respectively. An increase of $h_{po}$ attenuates the reduction of p in undrained conditions (because $D$ decreases) and therefore it increases the number of cycles required to reach 3% of shear strain. As a result, for increasing values of $h_{po}$ the cyclic resistance curve tends to be stretched towards the right part of the plot. On the contrary, when $C_\varepsilon$ is increased, the dilatant behavior of the soil is attenuating (i.e. $D$ decreases), thus requiring less cycles to reach $3\%$ of shear strain.

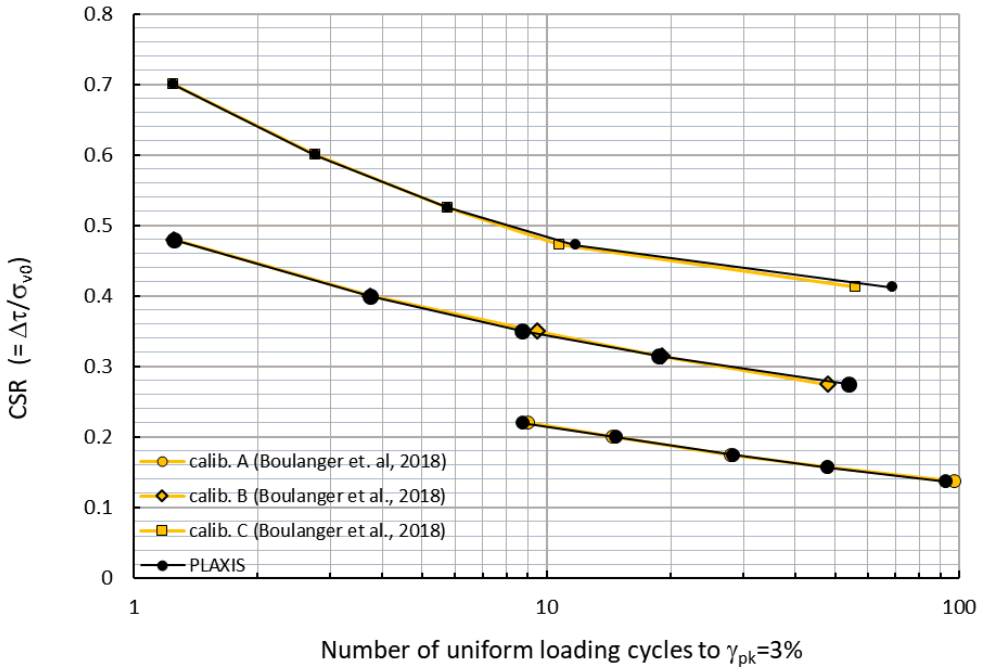


Figure 16*: CSR-N curves for calibrations A, B, C (data after Boulanger et al. (2018))*.

*Table 2. List of initial conditions to simulate cyclic undrained DSS tests to obtain the CSR plotted in* Figure 16*. In green are marked the tests shown in Figs. 15 and 16, respectively.*

| | Test | $\sigma'_{y0}$ | $\Delta\tau_{xy}$ | CSR | CSR/$S_{u,ratio}$ | K0 | # of cycles | # of steps per quarter |
|---|---|---|---|---|---|---|---|---|
| | | [ kPa ] | [ kPa ] | - | - | - | | |
| A | 1 | 101.3 | 13.93 | 0.1375 | 0.55 | 0.5 | 92.25 | 1000 |
| | 2 | 101.3 | 15.95 | 0.1575 | 0.63 | 0.5 | 47.75 | 1000 |
| | 3 | 101.3 | 17.73 | 0.175 | 0.7 | 0.5 | 28.25 | 1000 |
| | 4 | 101.3 | 20.26 | 0.2 | 0.8 | 0.5 | 14.75 | 1000 |
| | 5 | 101.3 | 22.29 | 0.22 | 0.88 | 0.5 | 8.75 | 1000 |
| | | | | | | | | |
| B | 1 | 101.3 | 27.86 | 0.275 | 0.55 | 0.5 | 53.75 | 1000 |
| | 2 | 101.3 | 31.91 | 0.315 | 0.63 | 0.5 | 18.75 | 1000 |
| | 3 | 101.3 | 35.455 | 0.35 | 0.7 | 0.5 | 8.75 | 1000 |
| | 4 | 101.3 | 40.52 | 0.4 | 0.8 | 0.5 | 3.75 | 1000 |
| | 5 | 101.3 | 48.624 | 0.48 | 0.96 | 0.5 | 1.25 | 1000 |
| | | | | | | | | |
| C | 1 | 101.3 | 41.79 | 0.4125 | 0.55 | 0.5 | 68.75 | 1000 |
| | 2 | 101.3 | 47.86 | 0.4725 | 0.63 | 0.5 | 11.75 | 1000 |
| | 3 | 101.3 | 53.1825 | 0.525 | 0.7 | 0.5 | 5.75 | 1000 |
| | 4 | 101.3 | 60.78 | 0.6 | 0.8 | 0.5 | 2.75 | 1000 |
| | 5 | 101.3 | 70.91 | 0.7 | 0.93 | 0.5 | 1.25 | 1000 |

## 4.2. Normalized shear modulus reduction and damping ratio curves from PLAXIS SoilTest simulations

Strain-controlled undrained CDSS tests are often performed to characterize the trend of the normalized secant shear modulus and equivalent damping ratio with respect to the maximum cyclic shear strain amplitude. To obtain these curves, several strain-controlled CDSS tests are performed by enforcing at each cycle of loading a given increment of shear strain $\Delta\gamma_{xy}$ which will be increased at the next cycle. Following this procedure, it is possible to calculate the Equivalent Secant Shear Modulus (ESSM) and Damping Ratio (DR) at each cycle, thus having the entire evolution of these variables in correspondence to the applied shear strain. An example of the shear modulus decay and equivalent damping ratio is shown in Figure 17 by using the calibration C reported in Table 1, and the following initial conditions: $|\sigma_{yy}| = 101.3$ kPa, $K_o = 0.5$.

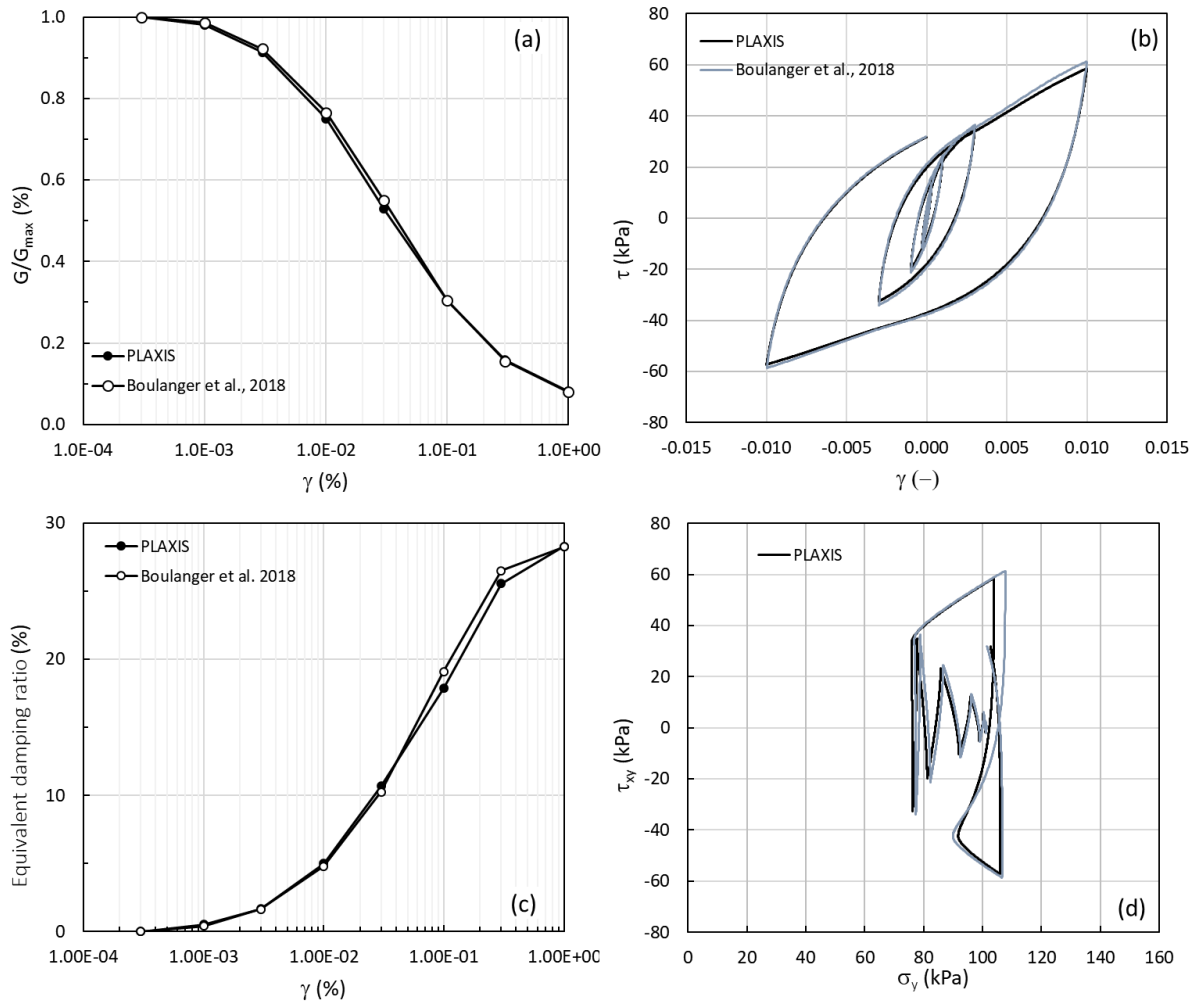


Figure 17. *Undrained strain-controlled CDSS tests for calibration C: (a) Shear modulus reduction curves, (b) stress-strain curves, (c) equivalent damping ratio curves, (d) effective stress paths.*

The results required to plot Figure 17 can be obtained by running several simulations in the tab "CDSS" of the PLAXIS SoilTest facility or preferably using the tab "General" through which a general stress path can be solved. An example of how solving an undrained cyclic DSS test withing the tab "General" is shown in Figure 18 where the horizontal stresses $\sigma_{xx}$ and $\sigma_{zz}$ have been assigned equal to $|\sigma_{xx}| = |\sigma_{zz}| = 50.15\ kPa$ to prescribe $K_o = 0.5$. As the test is controlled by enforcing the shear strain, a loop of loading is completed after the following three phases:

- Phase 1: $\Delta\gamma_{xy}$ represents the first increment of shear strain applied to the sample;
- Phase 2: it is applied $-2\Delta\gamma_{xy}$ to enforce the opposite amount of cumulated shear strain;
- Phase 3: $\Delta\gamma_{xy}$ is finally applied to reach the stage of zero total shear strain end complete a loop.

After these three phases, a further loop composed of three new phases can be defined to simulate multiple cycles and describe the full trend of shear modulus decay and damping ratio.

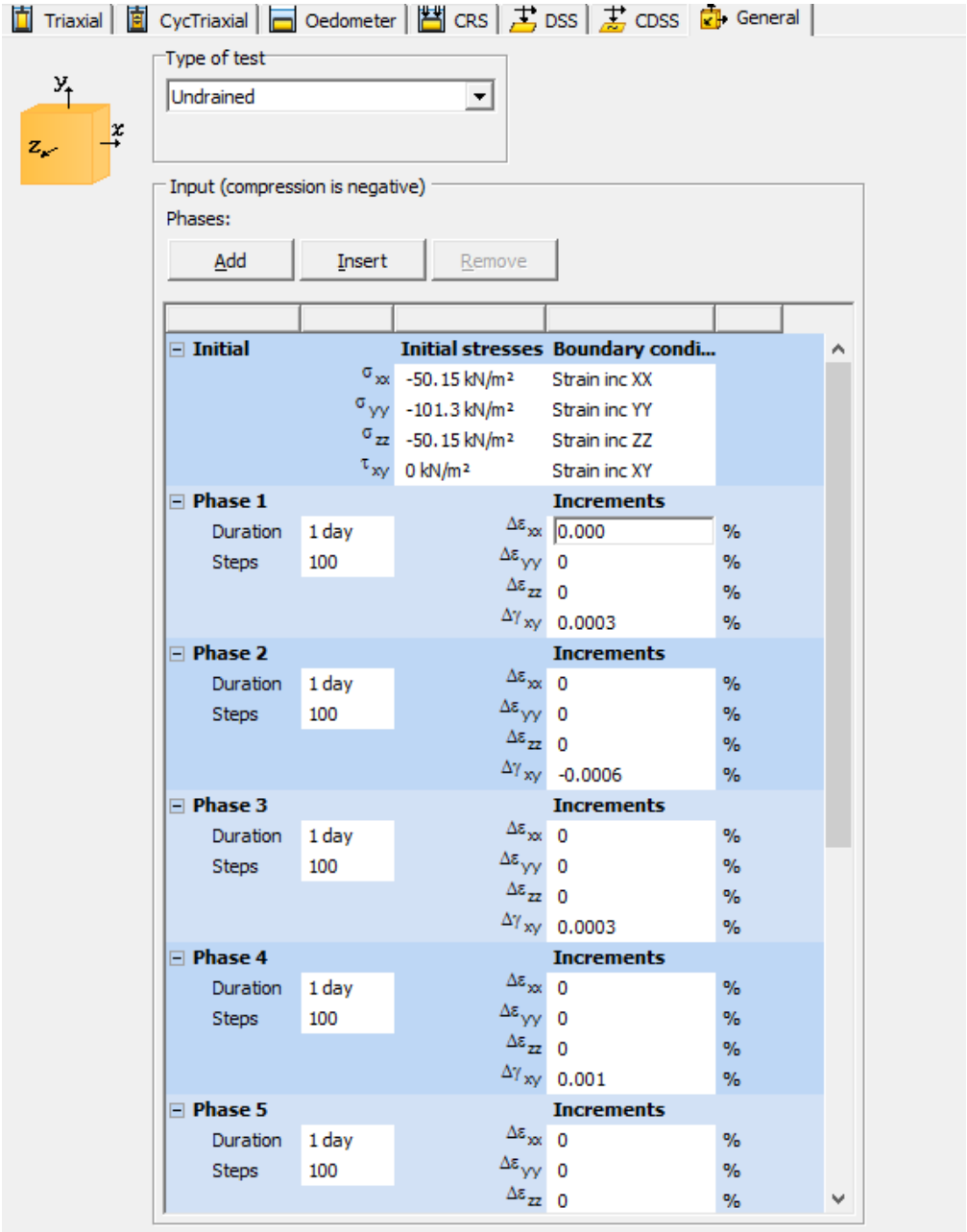


Figure 18. *PLAXIS SoilTest General tab to perform undrained strain-controlled CDSS tests: shear modulus reduction curve and equivalent stress-strain response for default calibration C.*

# 5. A 1D site response analysis

This section discusses the results of the seismic analysis of a soil deposit using PM4Silt to illustrate some features of the model and how to use it in PLAXIS 2D. The use of some output state variables to interpret the results and some practical indications for setting up the analysis are also provided. In this analysis, the set of parameters A presented in Table 1 is considered to model the mechanical behavior of a normally consolidated silty clay stratum (yellow layer of Figure 19) which extends to a depth of 29m and is delimited at the bottom by an elastic bedrock (green layer of Figure 19). The groundwater table is located two meters below the ground surface. The input motion chosen for the analysis is the time history of horizontal acceleration shown in Figure 20. At the base of the model, a compliant base boundary condition has been assigned to simulate the presence of an indefinite extension of the bedrock while along the vertical sides, tied degree boundary conditions are applied.

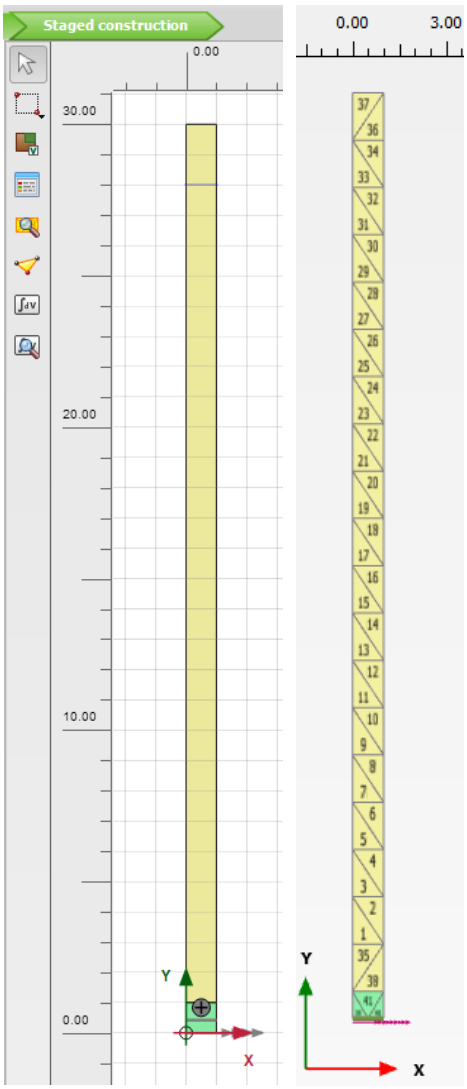


Figure 19. *Soil column model for the site response analysis of a silty clay deposit. Initial and boundary conditions and the resulting mesh discretization obtained by setting 1 to the coarseness factor on the sides of the column and choosing a medium mesh in PLAXIS Input*

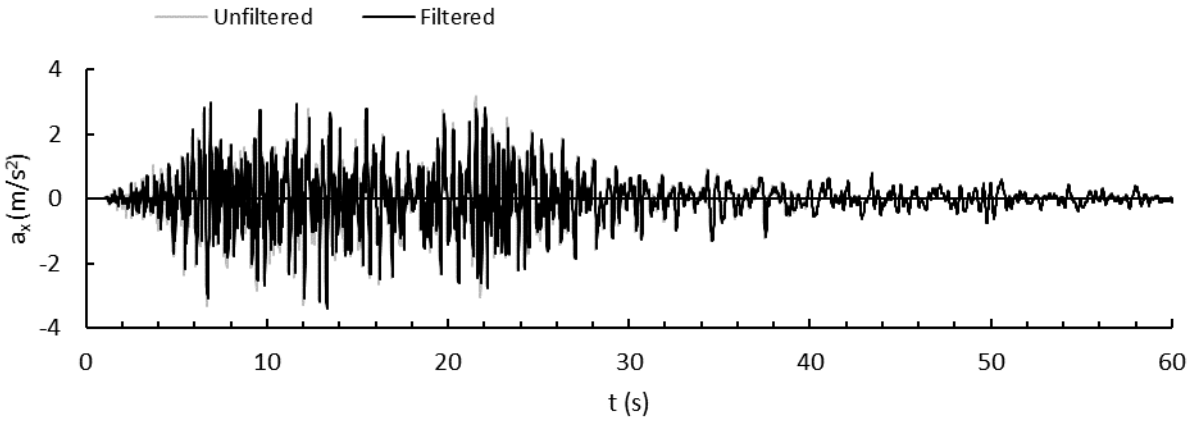


Figure 20. *Filtered and unfiltered time history of the input horizontal acceleration* ***(the filtered input record is separately provided through the file Acceleration_input_record.txt, showing a peak acceleration of -3.144 m/s )***

The accelerogram in Figure 20 has been obtained by scaling with a coefficient 2 a real recorded time history for which the maximum acceleration was 0.169g. This modification allows the model to achieve the mobilization of high shear strain levels in the soil column and to illustrate some specific features like the use of the state variables provided in output.

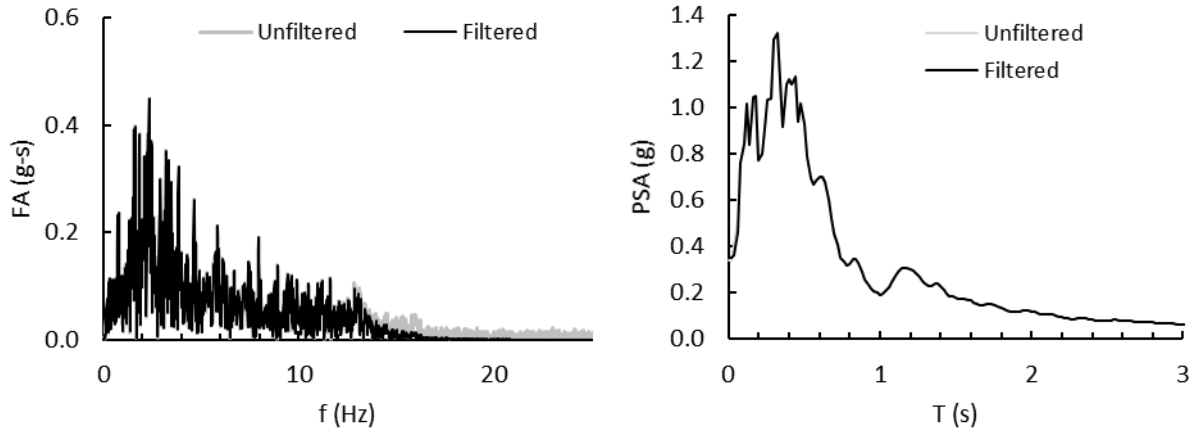


Figure 21. *Horizontal time history acceleration: filtered and unfiltered (a) Fourier amplitude spectrum, (b) Pseudo Spectral Accelerations (PSA).*

To avoid an alteration of the numerical results due to high frequencies, a Butterworth-type low-pass filter of order 8 with a cutoff frequency of 14Hz has been applied to remove frequencies higher than 18Hz. The final displacement drift at 60s is around 0.03m and, despite this being relatively small, the drift correction option has been selected in the analyses. The corrected and uncorrected signals are shown in both Figure 20 and Figure 21 and the unaltered characteristics of the two signals are further shown in Figure 21 (b) by means of the PSA of the two accelerograms.

The measurement unit chosen for the analysis are [m], [kN], and [day] and the gravity acceleration is set to 9.81 m/s$^2$. The bulk modulus of the water has been set to 2 GPa to guarantee small volumetric strains. While the parameters used for PM4Silt are shown in Table 1 (i.e. calibration A), all the other properties employed in the analyses to characterize the soil stratum and the elastic bedrock are reported in Table 3. It is worth noting that, due to the use of kPa as the default measurement unit, the atmospheric pressure can be set to 0.

*Table 3. Additional input parameters for the two layers.*

| **INPUT PARAMETERS: Silty clay stratum** | **CALIBRATION** | **UNIT** |
|---|---|---|
| | **B** | |
| Drainage type | Undrained A | |
| $\gamma_{unsat}$ - unsaturated unit weight | 13.786 | $kN/m^3$ |
| $\gamma_{sat}$ - saturated unit weight | 18.432 | $kN/m^3$ |
| $\alpha$ - Rayleigh damping coefficient | 0.01256 | |
| $\beta$ - Rayleigh damping coefficient | 0.3185*E-3 | |
| $e_0$ - initial void ratio | 0.9 | |
| | | |
| **INPUT PARAMETERS: Elastic bedrock** | **CALIBRATION** | **UNIT** |
| | *Elastic bedrock* | |
| Drainage type | Undrained A | |
| $\gamma_{unsat}$-unsaturated unit weight | 20.00 | $kN/m^3$ |
| $\gamma_{sat}$-saturated unit weight | 20.00 | $kN/m^3$ |
| $\alpha$ - Rayleigh damping coefficient | 0.01256 | |
| $\beta$ - Rayleigh damping coefficient | 0.3185*E-3 | |
| $e_0$ - initial void ratio | 0.5 | |
| $E$ – Young's modulus | 4*E6 | $kPa$ |
| $\upsilon$ – Poisson's ratio | 0.2 | |

The saturated and dry density assumed for the soil are computed considering a void ratio and a specific gravity equal to $e_0 = 0.9$ and $G_s = 2.67$, respectively. A small amount of Rayleigh damping is considered to prevent numerical noises in the results and is recommended especially when a high level of strain is expected. Specifically, the Rayleigh damping coefficients $\alpha$ and $\beta$ are calibrated to have a small variability of the critical damping ratio (DR) for the frequencies characteristic of the earthquake as well as the natural frequency of the deposit. In this manner, the value of the DR can be approximated as a constant during the solution of the problem. In this application, the Rayleigh damping coefficients $\alpha$ and $\beta$ are given in Table 3 and they correspond to a minimum DR equal to $\xi_0 = 0.2\%$ for a frequency $f_0 = 1\text{Hz}$. As shown in Figure 22, this frequency corresponds to a minimum of the DR function and it is close to the natural frequency of the deposit estimated with the initial elastic shear stiffness, i.e. approximately equal to $f = 1.24\text{Hz}$.

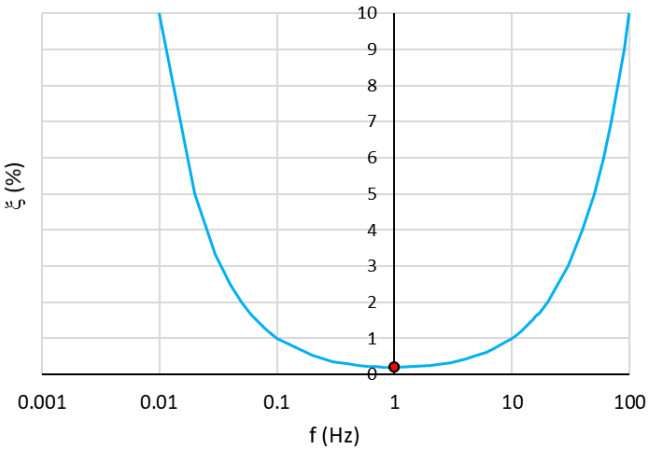


Figure 22*: Plot of the DR as a function of the frequency.*

As shown in Figure 23, the analysis is performed in two phases: (i) initial phase, calculation type "$K_o$ procedure", and (ii) Phase 1, calculation type "Dynamic". The first phase is used only to initialize the stress state with a $K_o = 0.5$, whereas the second is employed to solve the dynamic problem.

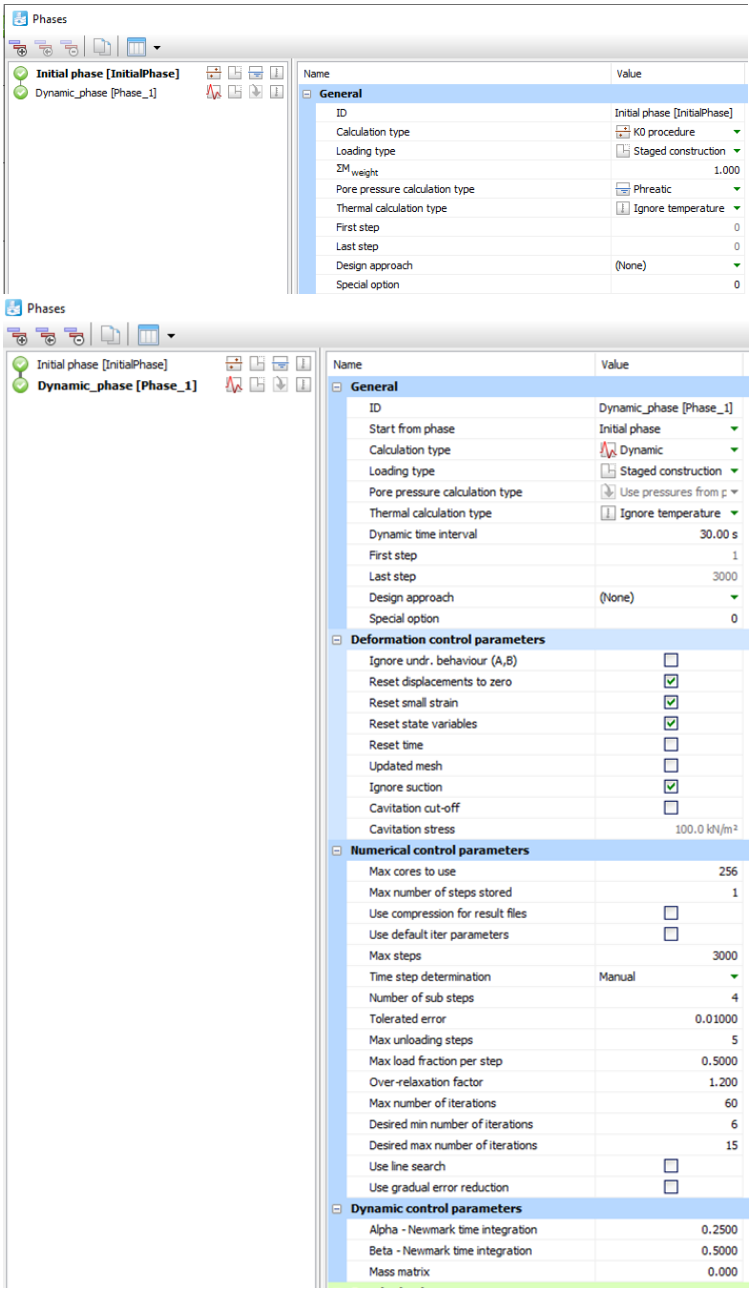


Figure 23*: PLAXIS Input screenshots of the phase settings for Initial phase and Phase 1.*

Although in the $K_o$ procedure the equilibrium equations are not solved, in this specific example the distribution of the effective stress is also balanced with the gravity loading, therefore it would not be necessary to reset the state variables at the beginning of the dynamic phase. As a matter of fact, parameters and state variables depending on the effective stress state are computed at the beginning of the first phase in which PM4Silt is used or when the reset of state variables is requested (see Section 3.1). If PM4Silt is used with the calculation type "Gravity loading procedure", where the initial effective stress is considered only as a first tentative, a reset of the state variables must be done before solving the dynamic problem thus avoiding the use of wrong parameters and state variables. The incorrect initialization could also generate potential numerical issues due to unrealistic values of the state variables. In some circumstances can therefore be useful to perform the static calculation type "Gravity loading procedure" with a simpler constitutive model (for example elastic perfectly plastic) for the soil to achieve an equilibrated effective stress distribution and then inserting a plastic nil-phase

before the dynamic phase in which the PM4Silt material is assigned to the soil deposit. Following this approach, it is then not necessary to reset the state variables before performing the dynamic analysis. After the change of constitutive models or after a reset of the state variables, the BCI state variable can be plotted to check if the initial effective stress state was violating the bounding surface and therefore an internal and automatic correction of the stress state has been performed to restore the consistency with the bounding surface.

Some of the state variables remain constant after the initialization (see Section 3.2). All the other quantities are updated at each step of the calculation. Therefore, for example, a check of the initial stiffness distribution should be done in the plastic nil-phase or at the first step of the dynamic phase. The distribution of $G$ or $K$ can be plotted to double check the calibration of the parameters $G_0$ and $n^G$. The dominant frequency 1.24 Hz of the deposit has been computed by exporting, through a cross-section, the initial elastic stiffness, and by computing, using the saturated density, the shear wave velocity profile, and the equivalent value of the shear wave velocity of the deposit as $V_{s,eq} = \frac{\sum_i h_i/V_{s,i}}{H}$, H being the height of the deposit and $h_i$ and $V_{s,i}$ corresponding to the thickness and the associated value of the shear wave velocity at the specific depth, respectively.

As shown in Figure 23, the number of steps is set equal to the number of points of the input accelerogram to have the same definition of input and output time histories. Before running the analyses, two nodes have been selected in correspondence to the top and bottom of the model to be able to retrieve the entire history of accelerations.

The accelerations in Figure 20 have been considered as outcrop motions and applied with a scaling coefficient equal to 0.5 on the line displacement at the bottom of the model. Considering that the input was scaled by a factor of 2, it is evident that the results would have been the same directly applying the original natural accelerogram. The choice has been done to remark that, when a compliant base is used, only the upward component of the motion should be applied at the base, being equal to 0.5 the outcrop motion in the case of a record performed on a stiff bedrock.

## 1.2 Results

Figure 24 shows the accelerations predicted at the top and the base of the column on the preselected nodes. A de-amplification of the peak acceleration is observed. The amplification of the harmonic with a frequency smaller than 1.24Hz (see the Fourier's spectrum in Figure 25) is justified by an expected degradation of the stiffness. Although the input has been filtered, harmonics with frequencies higher than 18Hz are still generated during the computation, particularly in the top node. However, their influence on the results is moderate, as shown by the acceleration at the top, confirming the benefic effects of the Rayleigh damping and the filtering of the input.

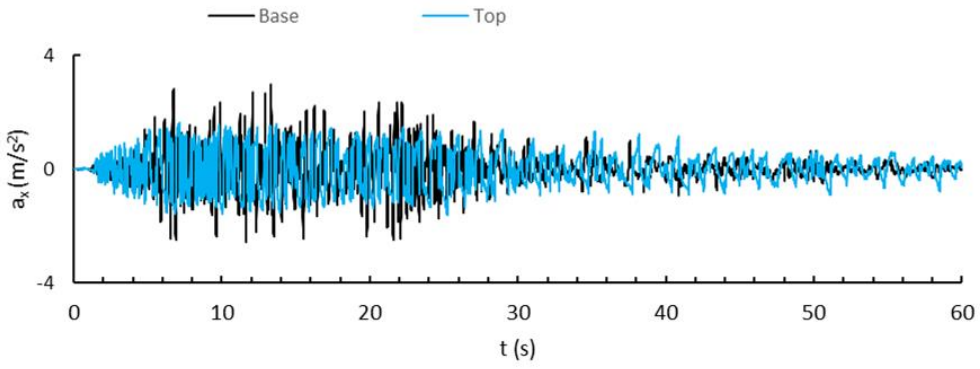


Figure 24. *Output of the horizontal acceleration history at the base and the top of the column.*

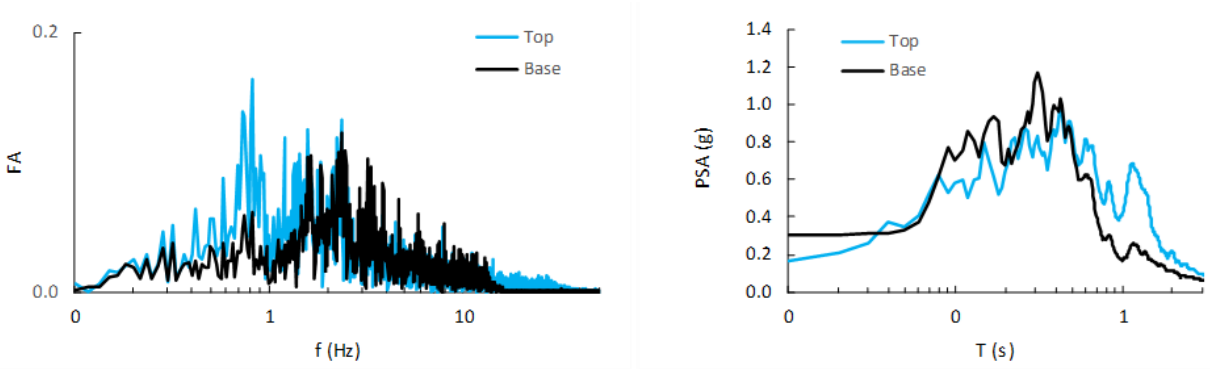


Figure 25. *Fourier (left) and Pseudo Acceleration Spectra (right) of the accelerations at the top and the base of the column.*

Figure 26 shows the distribution of the maximum accelerations and displacements reached during the first 30s of the analysis along a vertical cross-section in correspondence to the mid-line. An overall de-amplification is observed, which is in accord with the dissipative response of silts.

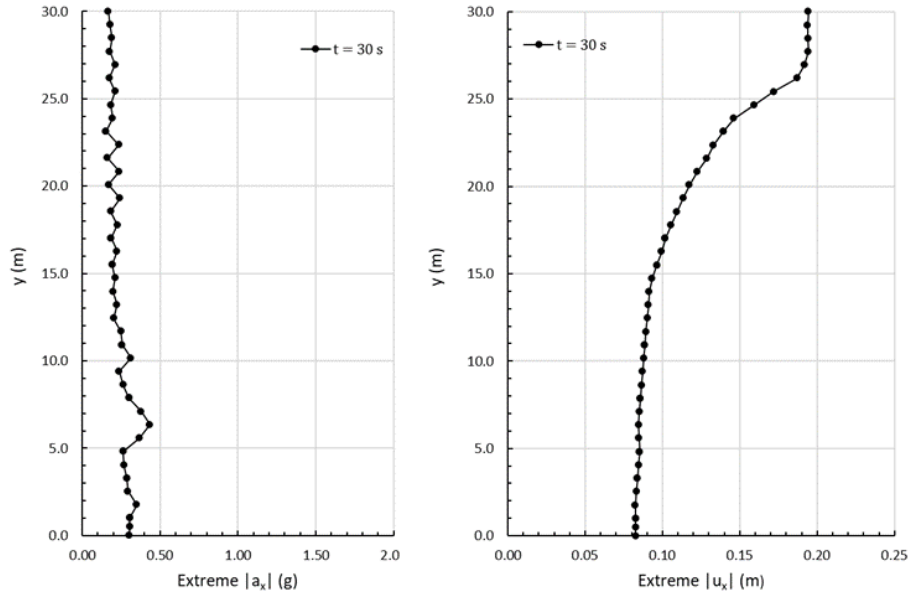


*Figure 26. Cross-section profiles of the maximum horizontal accelerations and displacements after 30s.*

In Figure 27 the cross-section of the state variables $\gamma/2_{MaxExtreme}$, $r_{u,Extreme}$ and $\tau_{xy,ratio,Extreme}$ are shown at the instant of Figure 26. In 2D boundary values problems, the iso-lines of $\gamma/2_{MaxExtreme}$ would represent the maximum deviatoric strains although, in the conditions of the analysis (undrained and one-dimensional), $\gamma/2_{MaxExtreme}$ coincides with $\varepsilon_{xy,Extreme}$. The results show localization of shear strains higher than 3% at 5m of depth associated to high values of $r_{u,Extreme}$.

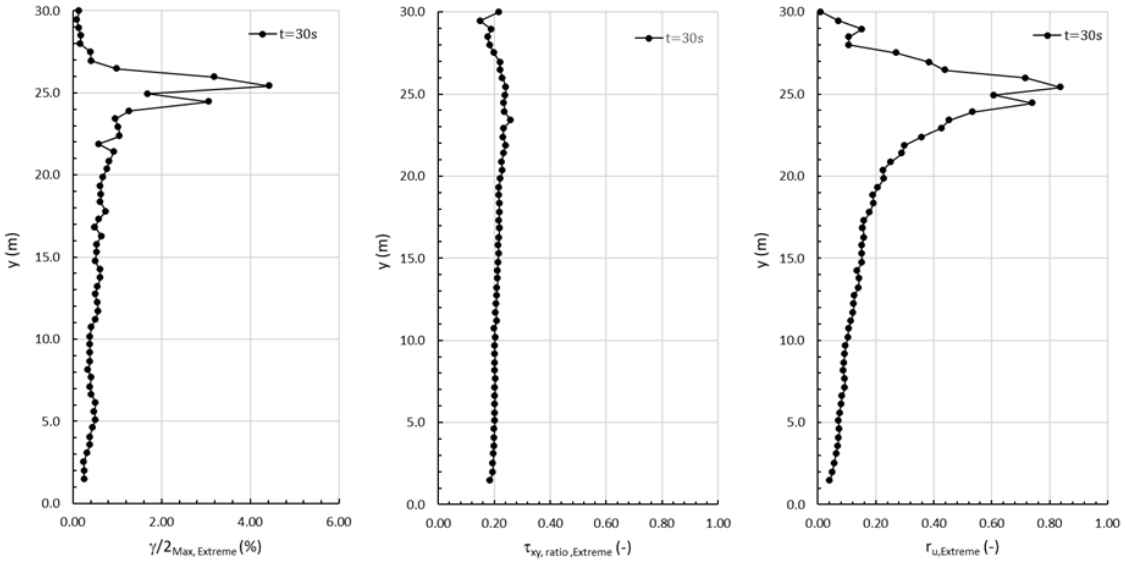


*Figure 27. Cross-section profiles of the three state variables after 30s.*

Looking at what is reported in Figure 28, the $Ipr$ close to one indicates that the highest value of $r_{u,Extreme}$ in Figure 27 coincides with $r_{u,Limit}$ (as shown in Figure 29, $r_{u,Limit}$ is 0.8427). Therefore, in the portion of the layer where the shear strains are greater than 3%, the minimum admissible mean effective stress has been reached**.** Note that $r_{u,max}$ in Figure 29 is equal to zero because the $p_{min}$ used to compute $r_{u,Limit}$ has been determined based on $S_{u,ratio}$.

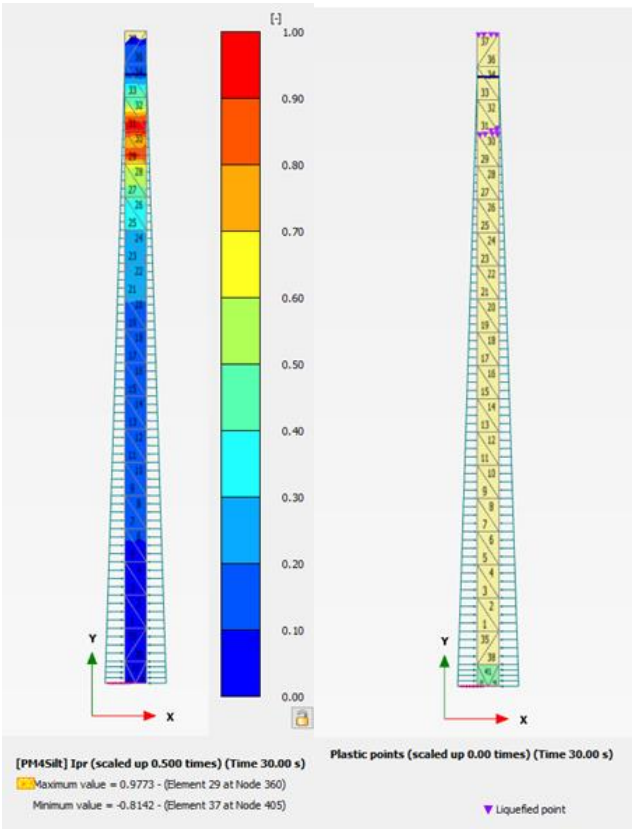


*Figure 28. Index of reduction of p and cyclic mobility ("Liquefied points") distributions.*

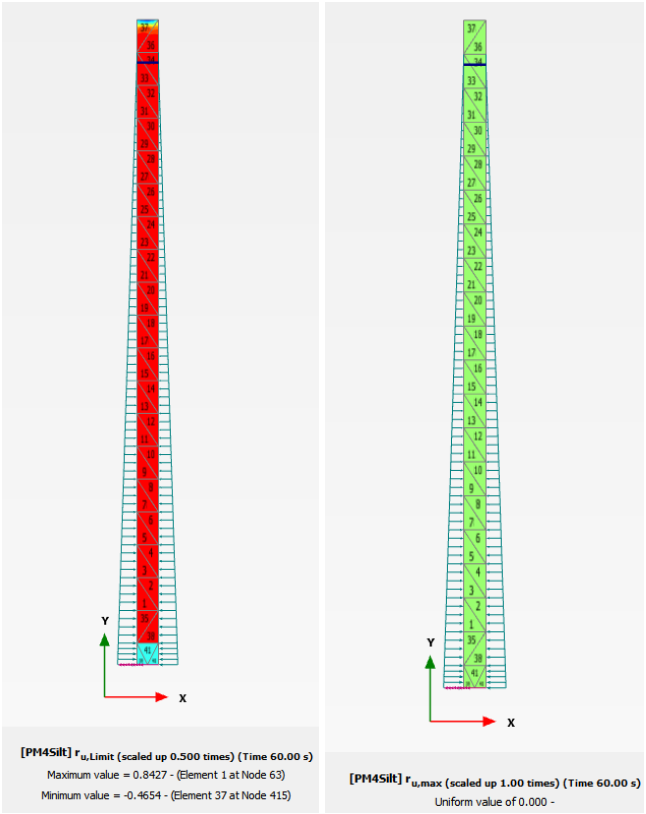


*Figure 29. Distributions of $r_{u,limit}$ and $r_{u,max}$ for the calibration A (Table 1).*

The results reported in the previous figures show that even if the level of the mean effective stress does not approach zero (the soil still retains ~80% of the initial mean effective stress), high levels of shear strains are mobilized and high levels of excess pore water pressure develop, indicating permanent damage and post shaking settlements in the deposit. The significant damage is quite localized for the case illustrated in this example, although worse conditions could be activated with initial static shear stresses, which also reduces the cyclic strength of the material (see Eq. 59). These results obtained for a lithostatic and very schematic condition indicate the importance of modeling the cyclic mobility and cyclic softening of clay-like soils and their peculiarities compared to the sand-like liquefaction (see for instance Tutorial 3 of the PLAXIS PM4Sand manual).

# 6. References


[1] Been, K. and Jefferies, M.G., 1985. A state parameter for sands. *Géotechnique*, *35*(2), pp.99-112.

[2] Boulanger, R.W. and Idriss, I.M., 2004. *Evaluating the potential for liquefaction or cyclic failure of silts and clays* (p. 131). Davis, CA: Center for Geotechnical Modeling.

[3] Boulanger, R.W. and Idriss, I.M., 2006. Liquefaction susceptibility criteria for silts and clays. *Journal of geotechnical and geoenvironmental engineering*, *132*(11), pp.1413-1426.

[4] Boulanger, R.W. and Idriss, I.M., 2007. Evaluation of cyclic softening in silts and clays. *Journal of geotechnical and geoenvironmental engineering*, *133*(6), pp.641-652.

[5] Boulanger, R.W. and Ziotopoulou, K., 2017. PM4Sand (Version 3.1): A sand plasticity model for earthquake engineering applications. *Center for Geotechnical Modeling Report No. UCD/CGM-17/01, Department of Civil and Environmental Engineering, University of California, Davis, CA*.

[6] Boulanger, R.W., Moug, D.M., Munter, S.K., Price, A.B. and DeJong, J.T., 2016. Evaluating liquefaction and lateral spreading in interbedded sand, silt, and clay deposits using the cone penetrometer. *Australian Geomechanics Society* Geotechnical and Geophysical Site Characterisation 5, B. M. Lehane, H. Acosta-Martinez, and R. Kelly, eds., Sydney, Australia, ISBN 978-0-9946261-2-7.

[7] Boulanger, R.W. and Ziotopoulou, K., 2018. PM4Silt (Version 1): A silt plasticity model for earthquake engineering applications. *Report No. UCD/CGM-18/01, Center for Geotechnical Modeling, Department of Civil and Environmental Engineering, University of California, Davis, CA.*

[8] Boulanger, R.W. and Wijewickreme, D., 2019, October. Calibration of a constitutive model for the cyclic loading response of Fraser River Delta Silt. In *Earthquake Geotechnical Engineering for Protection and Development of Environment and Constructions: Proceedings of the 7th International Conference on Earthquake Geotechnical Engineering,(ICEGE 2019), June 17-20, 2019, Rome, Italy* (p. 121). CRC Press.

[9] Boulanger, R.W. and Ziotopoulou, K., 2019. A constitutive model for clays and plastic silts in plane-strain earthquake engineering applications. *Soil Dynamics and Earthquake Engineering*, *127*, p.105832.

[10] Boulanger, R.W., 2019. Nonlinear Dynamic Analyses of Austrian Dam in the 1989 Loma Prieta Earthquake. *Journal of Geotechnical and Geoenvironmental Engineering*, *145*(11), p.05019011.

[11] Dafalias, Y.F. and Manzari, M.T., 2004. Simple plasticity sand model accounting for fabric change effects. *Journal of Engineering mechanics*, *130*(6), pp.622-634.

[12] Dahl, K.R., DeJong, J.T., Boulanger, R.W., Pyke, R. and Wahl, D., 2014. Characterization of an alluvial silt and clay deposit for monotonic, cyclic, and post-cyclic behavior. *Canadian Geotechnical Journal*, *51*(4), pp.432-440.

[13] Duncan, J.M., Wright., 2005. *Soil strength and slope stability*. New York Wiley.

[11] Jefferies, M.G. and Been, K., 2015. *Soil liquefaction: a critical state approach*. CRC press.

[15] Ladd, C.C. and Foott, R., 1974. New design procedure for stability of soft clays. *Journal of Geotechnical and Geoenvironmental Engineering*, *100*(Proc Paper 10064).

[16] Ladd, C.C., 1991 *Stability evaluation during staged construction: 22th Terzaghi Lecture" Journal of Geotechnical Engineering ASCE (117 (4) 537-615.*

[17] Ladd, C.C. and DeGroot, D.J., 2004. *Recommended practice for soft ground site characterization: Arthur Casagrande Lecture*. Massachusetts Institute of Technology.

[18] Montgomery, J., Boulanger, R.W., Armstrong, R.J. and Malvick, E.J., 2014. Anisotropic Undrained Shear Strength Parameters for Nonlinear Deformation Analyses of Embankment Dams. In *Geo-Congress 2014: Geo-characterization and Modeling for Sustainability* (pp. 1294-1306).

[19] Price, A.B., Boulanger, R.W., DeJong, J.T., Parra Bastidas, A.M. and Moug, D., 2015, November. Cyclic strengths and simulated CPT penetration resistances in intermediate soils. In *6th International Conference on Earthquake Geotechnical Engineering* (Vol. 14).

[20] Price, A.B., DeJong, J.T. and Boulanger, R.W., 2017. Cyclic loading response of silt with multiple loading events. *Journal of Geotechnical and Geoenvironmental Engineering*, *143*(10), p.04017080.

[21] Romero, S. (1995). "The behavior of silt as clay content is increased." MS thesis, University of California, Davis.

[22] Sheahan, T.C., Ladd, C.C. and Germaine, J.T., 1996. Rate-dependent undrained shear behavior of saturated clay. *Journal of Geotechnical Engineering*, *122*(2), pp.99-108.

# APPENDIX

## A.1. Dilatancy expressions

### A.1.1 Dilating behavior

$D_{non-rot}$ and $D_{rot}$ in Eq. 47 and Eq. 48 are selected according to the following statement:

· if $(D_{non-rot} < D_{rot})$ then

$$D = D_{non-rot} \tag{A1. 1}$$

· elseif $(D_{non-rot} \geq D_{rot})$ then

$$D = D_{non-rot} + (D_{rot} - D_{non-rot}) \cdot \frac{\langle M^b - M^{cur} \rangle}{\langle M^b - M^{cur} + 0.01 \rangle}, \tag{A1. 2}$$

$M^{cur}$ being the current stress ratio $\eta$.

The parameter $A_d$ in the equations of $D_{rot}$ and $D_{non-rot}$ is expressed as

$$A_d = \frac{A_{do}(C_{zin2})}{\left(\frac{z_{cum}^2}{z_{max}}\right)\left(1 - \frac{\langle -\boldsymbol{z}:\boldsymbol{n} \rangle}{\sqrt{2} \cdot z_{peak}}\right)^3 (C_\varepsilon)^2 (C_{pzp})(C_{zin1})(C_{zin2}) + 1} \tag{A1. 3}$$

where $A_{do}$ and $C_\varepsilon$ are model parameters which for silts and clays should be selected in the range of 0.8 – 1.2 and 0.5 – 1.3, respectively. The other variables are defined as

$$C_{zin1} = 1 - exp\left(-2 \cdot \left|\frac{\boldsymbol{z_{in}}:\boldsymbol{n} - \boldsymbol{z}:\boldsymbol{n}}{z_{max}}\right|\right) \tag{A1. 4}$$

$$C_{zin2} = \left[1 + C_{zin1} \cdot \left(\frac{z_{cum} - z_{peak}}{3z_{max}}\right)\right] / \left[1 + 3C_{zin1} \cdot \left(\frac{z_{cum} - z_{peak}}{3z_{max}}\right)\right] \tag{A1. 5}$$

$$C_{pzp} = 1 / \left[1 + \left(2.5 \frac{p}{p_{zp}}\right)^5\right] \tag{A1. 6}$$

In the last equation $p_{zp}$ is defined as the mean stress at the time in which the product $p \cdot |\boldsymbol{z}|$ reaches its maximum value. To define the DF in case of soil dilation is necessary to define also the back-stress ratio tensor for the rotated dilatancy, that is

$$\boldsymbol{\alpha^{dR}} = \left[\frac{M^{dR} - m}{\sqrt{2}}\right]\boldsymbol{n}, \qquad M^{dR} = \frac{M^d}{C_{rot1}} \tag{A1. 7}$$

where $M^{dR}$ means a rotated stress ratio (i.e. a reduced inclination of $M^d$). $C_{rot1}$ is equal to

$$C_{rot1} = 1 + 2 \cdot \frac{\langle -\boldsymbol{z}:\boldsymbol{n} \rangle}{\sqrt{2} \cdot z_{max}} \cdot (1 - \langle C_{zin1} \rangle) \tag{A1. 8}$$

To ensure that the model will be dilative for mean stresses smaller than $2\,p_{min}$, an additional constraint on the DF is enforced, i.e.

$if\ (p \leq 2p_{min}\ \ and\ \ D < D_{min})\ then$:

$$D = -3.5A_{do}\langle M^b - M^d\rangle \cdot \left(\frac{2p_{min} - p}{p_{min}}\right). \qquad \text{A1. 9}$$

### A.1.2 Contracting behavior

The DF for contracting is expressed through the variables $C_{in}$, $C_{p,min}$, $C_{dz}$ and $C_{wet}$ whose expressions are

$$C_{in} = \frac{2}{\sqrt{2}} \cdot \frac{\langle \boldsymbol{z}:\boldsymbol{n}\rangle}{z_{max}} \qquad \text{A1. 10}$$

$$C_{dz} = \left[1 - \sqrt{2} \cdot C_{rot2} \cdot \left(\frac{z_{peak}}{z_{max}}\right)\right] \cdot \left(\frac{z_{max}}{z_{max} + z_{cum} \cdot C_{rot2}}\right) \qquad \text{A1. 11}$$

$$C_{rot2} = 1 - \frac{z_{peak}}{z_{cum} + \left(\frac{z_{max}}{100}\right)} \qquad \text{A1. 12}$$

$$C_{wet} = \frac{1}{\frac{1}{C_{wet1}} + \frac{1}{C_{wet2}}} \leq 1 \qquad C_{wet1} = 1 + \left[\frac{C_{w1}}{(\boldsymbol{\alpha^b} - \boldsymbol{\alpha}):\boldsymbol{n}}\right]^4 \qquad C_{wet2} = 1 + \left[\frac{1}{C_{w2}} \cdot \frac{\xi}{\lambda}\right]^2 \qquad \text{A1. 13}$$

where $C_{w1}$ and $C_{w2}$ are parameters equal to 0.02 and 0.1, respectively. The value of $C_{p,min}$ depends on the value of the mean stress according to the following conditions:

$$C_{p,min} = 0 \quad if \quad (p \leq 2p_{min}) \qquad \text{A1. 14}$$

$$C_{p,min} = 1 \quad if \quad (p > 8p_{min}) \qquad \text{A1. 15}$$

$$C_{p,min} = \frac{p - 2 \cdot p_{min}}{6 \cdot p_{min}} \quad otherwise \qquad \text{A1. 16}$$

## A.2. Anisotropic undrained strength for non-linear deformation analyses

In the current implementation of PM4Silt an undrained strength $S_u$ variable for every stress point can be considered. The method proposed by Montgomery et al. (2014) has been implemented. The sequence of computation performed in every single stress point is briefly recalled. A more detailed description of this method and examples of application can be found in Montgomery et al. (2014) and Boulanger (2019).

The undrained shear stress at failure is equated to the undrained resistance and computed as

$$S_u \equiv \tau_{ff,K_c} = \tau_{ff,(K_c=1)} + \left[\frac{\tau_{ff,(K_c=K_f)} - \tau_{ff,(K_c=1)}}{K_f - 1}\right](K_c - 1)\,, \qquad A.2.\ 1$$

where $K_c$ is the consolidation stress ratio (i.e. $K_c = \sigma_{1c}/\sigma_{3c}$, with $\sigma_{1c}$ and $\sigma_{3c}$ the maximum and minimum principal stresses at consolidation) whereas $K_f$ is the stress ratio at failure (i.e. $K_f = \sigma_{1f}/\sigma_{3f}$, with $\sigma_{1f}$ and $\sigma_{3f}$ the maximum and minimum principal stresses at failure). The shear stress on the eventual failure planes $\tau_{ff}$ for consolidation at $K_c = 1$ and $K_c = K_f$ is computed by

$$\tau_{ff,K_c=1} = d_R + \sigma_{fc} \cdot tan(\psi_R)\,, \qquad A.2.\ 2$$

$$\tau_{ff,(K_c=K_f)} = c_c + \sigma_{fc} \cdot tan(\phi_c)\,. \qquad A.2.\ 3$$

where $c_c$, $\phi_c$, $d_R$ and $\psi_R$ are the parameters to be calibrated via ICUTX tests, while $K_c$ and $K_f$ are calculated internally from the principal stresses at consolidation and failure, corresponding to

$$\sigma_{1c} = \left(\frac{\sigma_v - \sigma_h}{2}\right) + \left[\left(\frac{\sigma_v - \sigma_h}{2}\right)^2 + \tau_{vh}\right]^{\frac{1}{2}}, \qquad A.2.\ 4$$

$$\sigma_{3c} = \left(\frac{\sigma_v - \sigma_h}{2}\right) - \left[\left(\frac{\sigma_v - \sigma_h}{2}\right)^2 + \tau_{vh}\right]^{\frac{1}{2}}, \qquad A.2.\ 5$$

and

$$\sigma_{1f} = \frac{\tau_{ff} - c'}{tan(\phi')} + \tau_{ff} tan(\phi') + \frac{\tau_{ff}}{cos(\phi')}\,, \qquad A.2.\ 6$$

$$\sigma_{3f} = \frac{\tau_{ff} - c'}{tan(\phi')} + \tau_{ff} tan(\phi') - \frac{\tau_{ff}}{\cos(\phi')}, \qquad A.2.\ 7$$

respectively. In the previous equations, the parameters $c'$ and $\phi'$ coincide with $\phi_c$ and $c_c$, respectively, as explained in Section 2.1.